

The Occurrence of Forsterite and Highly Oxidizing Conditions in Basaltic Lavas from Stromboli Volcano, Italy

JOAQUÍN A. CORTÉS^{1*}, MARJORIE WILSON¹, ERIC CONDLIFFE¹
AND LORELLA FRANCALANCI²

¹SCHOOL OF EARTH AND ENVIRONMENT (EARTH SCIENCES), UNIVERSITY OF LEEDS, LEEDS LS2 9JT, UK

²DIPARTIMENTO DI SCIENZE DELLA TERRA, UNIVERSITÀ DEGLI STUDI DI FIRENZE, VIA LA PIRA,
4, I-50121 FIRENZE, ITALY

RECEIVED FEBRUARY 16, 2005; ACCEPTED FEBRUARY 15, 2006;
ADVANCE ACCESS PUBLICATION MARCH 22, 2006

We report the occurrence of unusual, high-magnesium (Fo₉₆) olivine phenocrysts in a basaltic lava and an ejected lithic block from the Upper Vancori period (~13 ka) and the recent activity (2002–2003) of Stromboli volcano, Italy. The samples that contain this distinctive mineral chemistry are a shoshonitic basalt and a basaltic andesite with anomalous bulk-rock chemical characteristics in which the iron is highly oxidized (6–8 wt % Fe₂O₃ and <1 wt % FeO). In other respects these samples are similar to the majority of Stromboli basalts, characterized by the coexistence of olivine, clinopyroxene, plagioclase and Fe–Ti oxides as phenocrysts, and clinopyroxene, plagioclase and Fe–Ti oxides in the groundmass. In the high-magnesium olivine samples, Fe–Ti oxides (pseudobrookite) typically occur as symplectitic intergrowths with the olivine phenocrysts, indicating simultaneous growth of the two phases. We propose, as a paragenetic model, that the Fo₉₆ olivine phenocrysts crystallized from a highly oxidized basaltic magma in which most of the iron was in the ferric state; hence, only magnesium was available to form olivine. The highly oxidized state of the magma reflects sudden degassing of volatile phases associated with instantaneous, irreversible, transient degassing of the magma chamber; this is postulated to occur during periods of sudden decompression induced by fracturing of the volcanic edifice associated with paroxysmic activity and edifice collapse.

KEY WORDS: Stromboli; Mg-rich olivine; oxygen fugacity; redox state of magmas; irreversible processes

INTRODUCTION

Olivine is a ubiquitous phenocryst phase in basic and ultrabasic magmas with compositions typically in the range Fo_{91–88} (Deer *et al.*, 1997a; Cressey & Howie, 2005). Here, we report the unusual occurrence of highly magnesian olivine phenocrysts (Fo₉₆) in a shoshonitic basalt and a basaltic andesite lithic block from the prehistoric (Upper Vancori period) and recent (2002–2003) eruptive activity, respectively, of Stromboli volcano, Italy.

In the normal Stromboli mafic magmas, olivine phenocrysts typically vary from Fo₇₅ to Fo₈₂ in composition (Francalanci, 1993; Francalanci *et al.*, 2004); consequently, the presence of extremely magnesium-rich (>Fo₉₅) olivine phenocrysts requires an additional explanation. We propose that these anomalous olivine compositions are the products of crystallization from a highly oxidized melt in which oxidation is linked to transient and irreversible degassing of the magma chamber.

BACKGROUND TO THIS STUDY

Geological setting

Stromboli, a stratovolcano in the Tyrrhenian Sea, forms one of the islands of the Aeolian Arc (Fig. 1). For the past 2000 years it has exhibited persistent eruptive activity (Rosi *et al.*, 2000). General accounts of the chemistry and

*Corresponding author. Present address: Department of Geology, University at Buffalo, 876 Natural Sciences Complex, Buffalo, NY 14260-3050, USA. E-mail: caco@buffalo.edu

© The Author 2006. Published by Oxford University Press. All rights reserved. For Permissions, please e-mail: journals.permissions@oxfordjournals.org

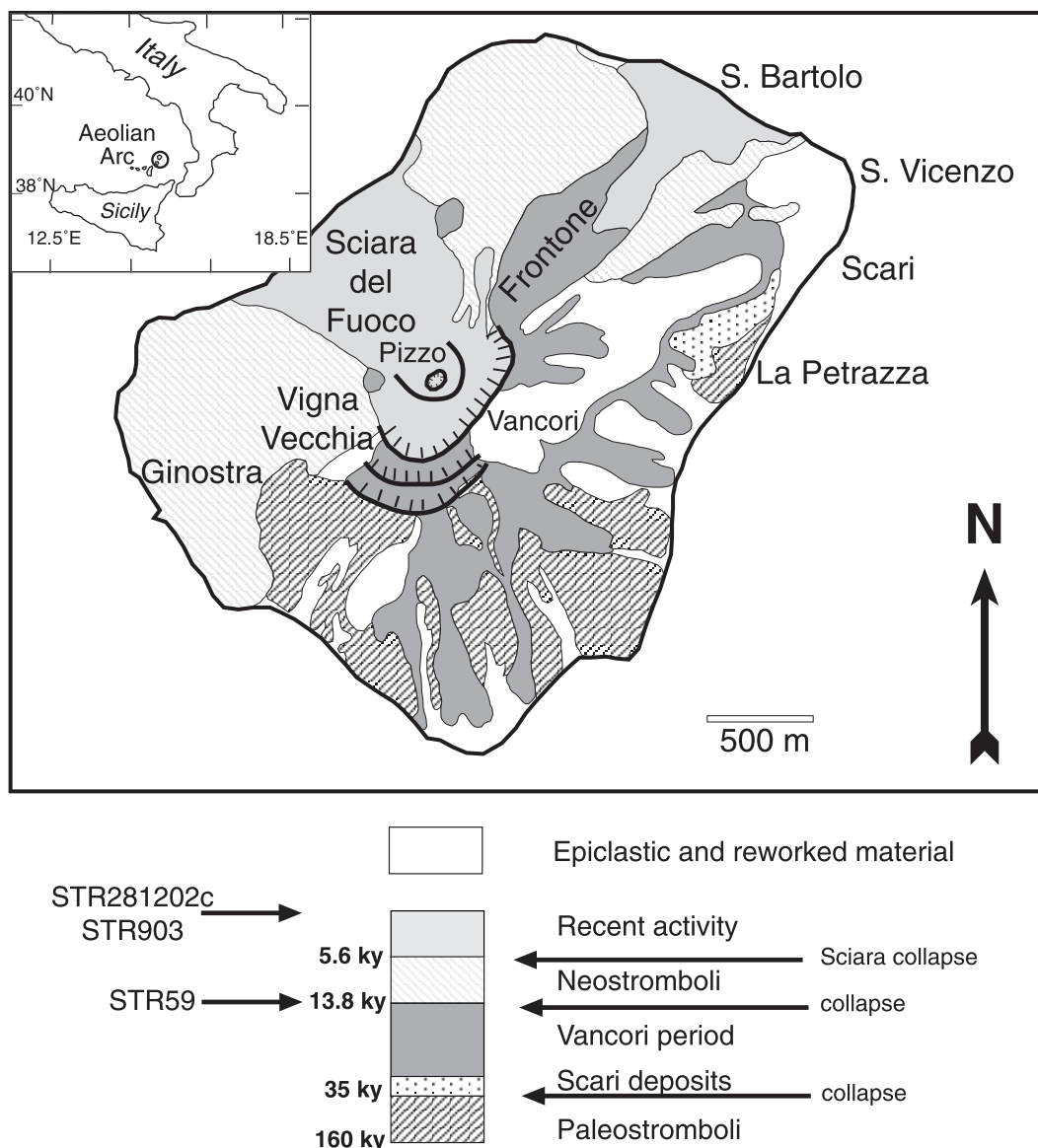


Fig. 1. Geological map of Stromboli simplified from Keller *et al.* (1993). The summary stratigraphic section of the volcano shows the relative ages of the highly oxidized samples (STR59, STR903) and the main periods of edifice collapse.

mineralogy of the eruptive products, and of the geological and tectonic setting, have been given by Francalanci *et al.* (1989, 2004), Ferrari & Manetti (1993), Hornig-Kjarsgaard *et al.* (1993), Keller *et al.* (1993), Tibaldi (2001), Tibaldi *et al.* (2003) and Arrighi (2004). The volcano has a volume of $\sim 300 \text{ km}^3$, and its subaerial part was built in the last 100 kyr through four main periods of activity: Paleostromboli (100–35 ka), the Vancori period (26–13.8 ka), Neostromboli (13.8–5.6 ka) and Recent (5.6 ka–present). These main divisions are defined largely by collapse episodes of the volcanic edifice (Fig. 1). The Vancori products filled the remnants of the Paleostromboli edifice, a caldera formed at the end of the

Paleostromboli period (Hornig-Kjarsgaard *et al.*, 1993). A lateral collapse at ~ 13.8 ka defines the end of the Vancori period (Vancori collapse, coaxial with the present-day Sciara del Fuoco scar), and the Neostromboli collapse, which occurred in the same direction at ~ 5.6 ka, defines the end of the Neostromboli period (Hornig-Kjarsgaard *et al.*, 1993; Tibaldi *et al.*, 1994, 2003; Tibaldi, 2001). Subsequently, a new vent became active in the area of Pizzo (Fig. 1), marking the onset of the Recent activity of the volcano. Following the Neostromboli collapse of the edifice, several smaller collapses have occurred in the same area, the last one in AD 1350 ± 60 (Arrighi, 2004), forming the Sciara del Fuoco in its

Table 1: Selected bulk-rock major element compositions (wt %) of lavas from various Stromboli periods

	Paleostromboli I STR79	Paleostromboli II STR38	Paleostromboli III STR164	Lower Vancori STR46	Middle Vancori STR53	Upper Vancori STR29	Neostromboli STR4	Recent STR24
SiO ₂	52.94	54.37	51.55	51.28	53.59	58.73	51.7	51.82
TiO ₂	0.79	0.78	0.93	0.9	1	0.7	0.9	0.78
Al ₂ O ₃	18.53	18.11	17.49	18.18	18.26	18.13	17.65	18.01
Fe ₂ O ₃	2.2	2.56	4.73	1.77	3.18	3.56	1.64	2
FeO	5.11	4.5	3.92	6.35	4.76	2.04	5.84	5.52
MnO	0.15	0.14	0.16	0.16	0.15	0.14	0.14	0.14
MgO	5.36	5.36	5.14	5.64	3.31	2.77	5.71	6.63
CaO	9.55	9.1	10.11	10.28	8.43	5.52	8.94	10.16
Na ₂ O	2.86	2.71	2.63	2.36	3.06	3.6	2.31	2.23
K ₂ O	1.8	1.76	1.95	2.12	2.69	3.93	4.41	1.79
P ₂ O ₅	0.21	0.31	0.32	0.37	0.54	0.29	0.51	0.23
LOI	0.43	0.24	1.01	0.52	0.98	0.55	0.2	0.63
Total	99.93	99.94	99.94	99.93	99.95	99.96	99.95	99.94

Data are from Francalanci *et al.* (1993).

present shape and resulting in a highly faulted volcanic edifice.

The composition of the erupted products (principally lavas, breccias and scoria bombs) is mainly basaltic to basaltic–andesitic, spanning the complete range of subduction-related magma series from calc-alkaline to shoshonitic; magma compositions have shifted periodically with time (Francalanci *et al.*, 1989; Horning-Kjarsgaard *et al.*, 1993). The activity of the Vancori and Recent periods of activity is shoshonitic, whereas the Neostromboli period products are richer in potassium (leucite-normative shoshonites) (Francalanci *et al.*, 1989, 1993). Representative bulk-rock chemical analyses of individual lava samples from the main volcanic periods, from Francalanci *et al.* (1993), are given in Table 1.

Strombolian activity and paroxysms

Stromboli is the type locality of Strombolian eruptions, which normally occur several times per hour from one or more of the active vents sited 150 m below the Pizzo Sopra la Fossa peak (Fig. 1). This style of activity is characterized by the intermittent explosion or fountaining of basaltic lava from the vents with scoria bombs, blocks, lapilli and ash ejected within a very restricted area close to the vents. Occasionally, and without clear precursors, the volcano enters a period of more vigorous activity, which can occur a few times a year. This kind of activity is called a ‘paroxysm’ (Barberi *et al.*, 1993). This is characterized by the ejection of the volcanic products outside the caldera rim of the Vancori volcano (Fig. 1). Bombs can even land on the villages on the island, as

happened in the paroxysmic activity of 1930 (Abruzzese, 1935) or in the last paroxysmic activity in April 2003 (Ripepe *et al.*, 2005).

Two main possibilities have been proposed to explain this kind of activity: changes in the volatile flux, or changes in the groundwater level. Recently it has been demonstrated that paroxysmic activity is heralded by anomalous increases in sulphur degassing (Aiuppa & Federico, 2004) and CO₂ and H₂ degassing (Carapezza *et al.*, 2004), strongly suggesting that the shift in the style of activity is mainly controlled by changes in the volatile flux. On the other hand, changes in the perched aquifer in the Fossa crater could also trigger a phreatomagmatic eruption (Revil *et al.*, 2004).

Geochemical characteristics of the Stromboli lavas and the occurrence of forsteritic olivine

Detailed studies of the bulk-rock chemistry of the Stromboli lavas have been published by Francalanci *et al.* (1989, 1993, 2004) and Horning-Kjarsgaard *et al.* (1993). These provide an internally consistent dataset (~290 analyses) of the Stromboli eruptives from the various periods of activity. Whereas the bulk-rock analyses of these samples were obtained by X-ray fluorescence (XRF), the Fe₂O₃ and FeO contents were determined separately (total iron as Fe₂O₃ by XRF and FeO by titration). Within this dataset we have observed that ~20% of the samples, mainly from the Upper Vancori and Neostromboli periods, have higher amounts of Fe₂O₃ than FeO. Petrographic and electron microprobe

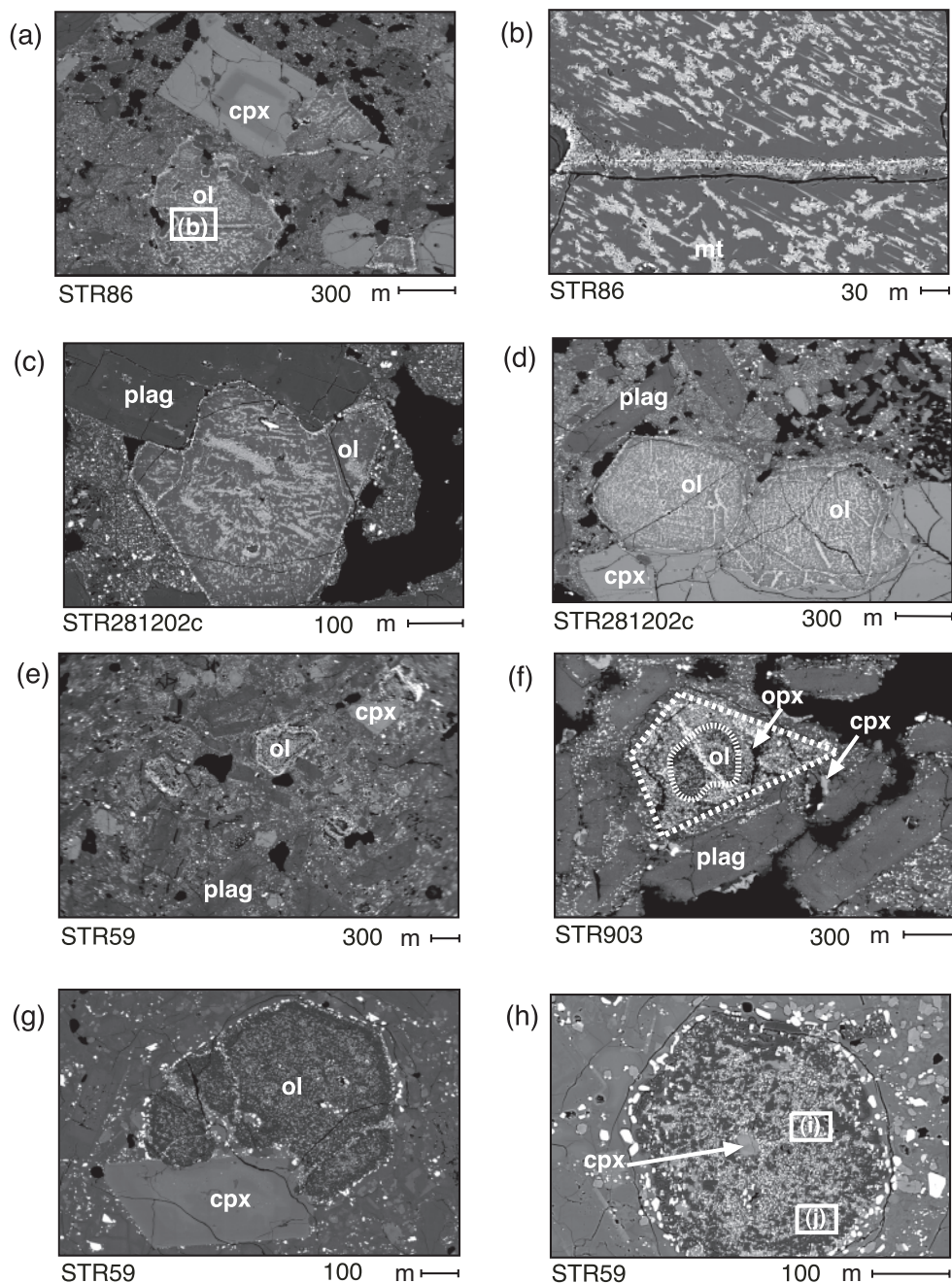


Fig. 2. (a) Back-scattered electron (BSE) image of sample STR86 showing zoned clinopyroxene (cpx) phenocrysts and sub-liquidus oxidized olivine phenocrysts (ol). (b) Enlarged BSE image of the sub-liquidus oxidized olivine from (a) showing bands of Fe-oxide (magnetite). The composition of the host olivine is Fo_{73} . (c) BSE image of sample STR281202c showing a sub-solidus oxidized olivine phenocryst (Fo_{82}). (d) BSE image of sample STR281202c showing a sub-solidus oxidized olivine phenocryst (Fo_{84}) in contact with normal diopsidic clinopyroxene. It should be noted that the oxidation in (c) and (d) is confined to cracks in the olivine phenocryst. (e) BSE image of sample STR59, showing the Mg-rich olivine (ol), clinopyroxene (cpx) and plagioclase (plag). (f) BSE image of Fo_{97} olivine (ol) with orthopyroxene reaction rim (opx) in sample STR903. The dashed lines highlight the boundaries of the phases. A small clinopyroxene phenocryst (cpx) and plagioclase phenocryst (plag) are also shown. (g) BSE image of Fo_{96} olivine (ol) intergrown with clinopyroxene (cpx) in sample STR59. (h) Clinopyroxene inclusion in a Mg-rich (Fo_{97}) olivine. Sample STR59. (i), (j) Vermicular symplectite-like texture of Fe–Ti oxides in sample STR59. Both are magnifications of parts of (h). (k) Photomicrograph of sample STR47, plane-polarized light, showing phenocrysts of olivine (ol), clinopyroxene (cpx) and plagioclase (plag) in a groundmass of olivine, clinopyroxene, plagioclase and Fe–Ti oxides. (l) The same field of view as in (k), under crossed polars. (m) Photomicrograph of sample STR59, showing phenocrysts of clinopyroxene (cpx), olivine (ol) and plagioclase (plag) in a groundmass of olivine, clinopyroxene, plagioclase and Fe–Ti oxides. (n) The same field of view as in (m), under crossed polars. A scale bar in microns shows the scale in all the figures.

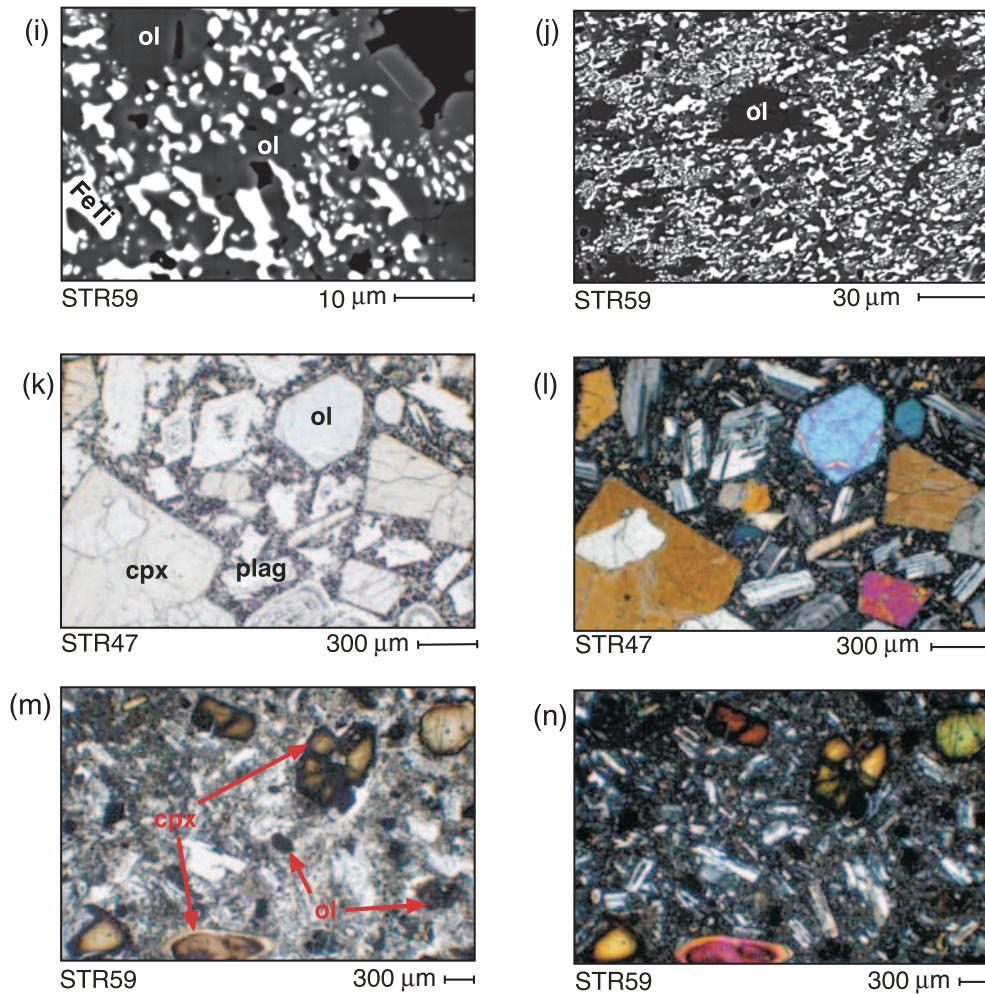


Fig. 2. Continued

studies of these high-Fe³⁺ samples suggest that, in almost all cases, the high amount of Fe₂O₃ is caused by oxidation of an olivine phenocryst-bearing magma (Fig. 2a and b). Depending on whether the oxidation process happened before or after the magma was completely solidified defines whether the oxidation is a sub-liquidus or sub-solidus process. Sub-liquidus oxidation can be distinguished from sub-solidus oxidation based upon the compositions of the groundmass phases. In both scenarios, normal Fo₇₇ olivine phenocrysts react to form magnetite and orthopyroxene, which are mainly constrained in bands within the host olivine (see discussion below). Evidence for sub-solidus oxidation in the first lava erupted in the 2002–2003 volcanic crisis (Ripepe *et al.*, 2005) was also found in our studies (sample STR281202c, Fig. 2c and d).

Among the oxidized samples studied, two samples (STR59, STR903) were found to have highly magnesian olivine phenocrysts (Fo₉₆); the bulk-rock analyses of these

samples have the highest amounts of Fe₂O₃ in the dataset. We demonstrate that this unusually forsteritic olivine is a consequence not of oxidation of pre-existing (normal) olivine phenocrysts, but of the growth of the olivine from a highly oxidized magma. These two samples form the focus of this study. We refer to them in subsequent discussions as ‘highly oxidized’, in comparison with the ‘normal’ (sub-solidus or sub-liquidus oxidized) Stromboli eruptive products.

SAMPLE SELECTION AND ANALYTICAL METHODS

Sample STR59 was collected from the boundary between the eruptives of the Upper Vancori period and those of the Neostromboli period, which is marked in the stratigraphic record by the Vancori collapse (Tibaldi *et al.*, 1994). This collapse event is represented in the field by the Frontone Breccias horizon (Hornig-Kjarsgaard *et al.*,

1993). The sample was collected from the first lava layer overlying the Frontone Breccias (Cortés *et al.*, 2005), thus representing the first erupted lava after the collapse of the Vancori edifice. Sample STR903 was collected in Ginostra (Fig. 1) from a block that was ejected during a major explosion on 5 April 2003. There is no way to tell, absolutely, whether or not the sample is juvenile (radiometric dating is not possible, as the likely age range is beyond the limit of detection of the Ar–Ar method). However, the person who collected the sample (D. Rothery, personal communication, 2005) is convinced that it is a juvenile fragment, as it does not show any evidence of alteration, unlike most of the other lithic blocks erupted in previous explosions. Additionally, the geochemical compositions of similar blocks have been determined and their Sr isotopic composition is comparable with that of the most recent activity of the volcano (L. Francalanci, unpublished data) rather than previous activity. Consequently, we propose that STR903 is a fragment of a solidified body of juvenile magma that had recently solidified within the main conduit of the volcano and was ejected during the paroxysmic explosion.

Based on the above scenario, sample STR903 must have solidified at some point between the opening of the fissure in the Sciara del Fuoco from which lava sample STR281202c was erupted on 28 December 2002 (Carapezza *et al.*, 2004; Ripepe *et al.*, 2005) and the 5 April 2003 explosion.

Sample STR281202c was collected at sea level from a very fast flowing lava that overflowed the northern rim of the NE summit crater on 28 December 2002. The lava overlies a pyroclastic deposit, emplaced during a short-lived mildly explosive episode that occurred just before the onset of lava effusion [equivalent to the ‘glowing lava’ of Carapezza *et al.* (2004)]. STR281202c has been interpreted as a sample of the magma that was filling the upper conduit prior to the onset of the 28 December eruption (Carapezza *et al.*, 2004; Ripepe *et al.*, 2005). Basalt samples (normal oxidation) STR47 (Lower Vancori) and STR4 (Neostromboli), taken from the dataset of Francalanci *et al.* (1989), were chosen as control samples to be representative of the shoshonitic series (Vancori) and the leucite-normative shoshonite series (Neostromboli), respectively. Sample STR86 (Neostromboli), from Francalanci *et al.* (1989) is an example of non-recent sub-liquidus oxidation.

The petrography of the samples was determined using a combination of optical microscopy and back-scattered electron imaging using a CamScan Series 4 electron microscope operated at 20 kV. Compositions of olivine, clinopyroxene, orthopyroxene, plagioclase and Fe–Ti oxides were determined using a Cameca SX-50 electron microprobe at the University of Leeds, fitted with three wavelength-dispersive spectrometers (used for all fully

quantitative analyses) and an Oxford MicroAnalysis Division Link 10/55S Energy Dispersive System (for reconnaissance and qualitative analysis). The amount of ferric and ferrous iron in the pyroxenes was estimated using the Papike charge-balance method following Lindsley (1983). For the Fe–Ti oxides in the highly oxidized samples, the assumption that all the iron is in the ferric state gives the best stoichiometry; the basis for this assumption is explained in further detail below. Representative mineral compositions are given in Tables 2–5; the complete dataset is available for downloading from <http://www.petrology.oxfordjournals.org/>.

Bulk-rock major element chemical analyses of samples STR903 and STR281202c were made at the Department of Earth Sciences of the University of Florence, Italy, using X-ray fluorescence (XRF) and wet chemical methods. MgO and Na₂O contents were determined by atomic absorption spectroscopy (AAS), and FeO contents by titration and loss on ignition (LOI) using gravimetric methods corrected for FeO oxidation during ignition. Bulk-rock major element chemical analyses of samples STR59, STR4 and STR86 were previously reported by Francalanci *et al.* (1989).

Rare earth element (REE) and trace element abundances in samples STR59 and STR903 were determined at the inductively coupled plasma mass spectrometry (ICP-MS) laboratory of the Department of Earth Sciences at the Open University (UK), using an Agilent 7500 s ICP-MS system. REE and trace element data for sample STR47 were reported by Cortés *et al.* (2005), and for STR4 and STR86 by Francalanci *et al.* (1989). REE and trace element abundances in sample STR28012c were determined by SGS Minerals Services of Toronto, Canada, by inductively coupled plasma atomic emission spectrometry (ICP-AES) and ICP-MS. The data are reported in Table 6.

PETROGRAPHY AND MINERAL CHEMISTRY OF THE STUDIED SAMPLES

For a detailed account of the mineral chemistry of the ‘normal’ Stromboli basalts the reader is referred to Francalanci (1993) and Cortés *et al.* (2005). For comparative purposes, we include in Tables 2–5 mineral chemical data for the control samples STR47 (Lower Vancori period) and STR4 (Neostromboli) as representatives of phenocrysts in the ‘normal’ Stromboli basalts.

Photomicrographs of both normal and oxidized basalt samples are included in Fig. 2 to show how the samples appear under a normal petrographic microscope. Figure 2k (plane-polarized light) and Fig. 2l (cross-polarized light) are photographs of sample STR47, a typical, shoshonitic basalt from the Vancori period.

Table 2: Selected electron microprobe analyses of olivine phenocrysts

	STR47	STR4	STR86	STR281202c	SRT59	SRT59	SRT59	SRT59	SRT59	STR903	STR903	STR903	STR903	STR903
	core	core	core	core	core	core	core	core	core	core	core	core	core	core
SiO ₂	36.43	38.12	40.02	39.73	42.20	42.31	42.46	42.97	41.71	42.46	42.47	42.80	42.55	42.92
TiO ₂	0.01	0.06	0.00	0.00	n.a.	0.01	0.01	0.03	0.05	0.03	n.a.	0.02	0.03	0.02
Al ₂ O ₃	n.a.	0.00	0.02	0.02	n.a.	0.04	0.03	0.13	0.04	0.03	0.09	0.04	n.a.	0.05
FeO	29.91	23.54	14.99	15.42	2.67	2.31	2.14	2.35	2.46	1.72	2.28	2.09	2.09	1.92
MnO	0.56	0.36	0.58	0.55	0.78	0.81	0.87	0.79	0.87	0.87	0.84	0.70	0.92	0.75
MgO	32.78	38.09	44.86	44.24	54.20	54.37	54.46	53.42	54.55	54.57	54.22	54.44	54.94	54.30
CaO	0.39	0.27	0.12	0.12	0.12	0.12	0.13	0.22	0.15	0.04	0.02	0.03	0.03	0.03
NiO	n.a.	0.10	0.05	0.09	0.04	0.05	0.03	0.04	0.10	0.04	0.07	0.06	n.a.	0.14
Total	100.08	100.53	100.63	100.18	100.01	100.02	100.14	99.95	99.92	99.76	99.97	100.17	100.57	100.13
<i>Cations per 4 oxygens</i>														
Si	0.98	0.99	1.00	1.00	1.00	1.00	1.01	1.02	0.99	1.01	1.01	1.01	1.00	1.01
Ti	0.00	0.00	0.00	0.00	n.a.	n.a.	n.a.	n.a.	n.a.	n.a.	n.a.	n.a.	n.a.	n.a.
Al	n.a.	0.00	0.00	0.00	n.a.	n.a.	n.a.	n.a.	n.a.	n.a.	n.a.	n.a.	n.a.	n.a.
Fe ²⁺	0.68	0.51	0.31	0.32	0.05	0.05	0.04	0.05	0.05	0.03	0.05	0.04	0.04	0.04
Mn	0.01	0.01	0.01	0.01	0.02	0.02	0.02	0.02	0.02	0.02	0.02	0.01	0.02	0.02
Mg	1.32	1.48	1.67	1.66	1.92	1.92	1.92	1.89	1.94	1.93	1.92	1.92	1.93	1.91
Ca	0.01	0.01	0.00	0.00	0.00	0.00	n.a.	0.01	n.a.	n.a.	n.a.	n.a.	n.a.	n.a.
Ni	n.a.	0.00	0.00	0.00	n.a.	n.a.	n.a.	n.a.	n.a.	n.a.	n.a.	n.a.	n.a.	n.a.
Total	3.01	3.01	3.00	3.00	3.00	3.00	2.99	2.98	3.00	2.99	2.99	2.99	3.00	2.98
%Fo	65.73	73.97	83.70	83.16	96.54	96.88	96.98	96.79	96.68	97.40	96.87	97.20	97.00	97.30

Analyses are in wt % and cations per formula unit (c.f.u.) recalculated on the basis of four oxygens in samples STR59 and STR903. Additional analyses are given for control samples (STR47, STR4) and sub-solidus and sub-liquidus oxidized samples (STR86, STR281202c). n.a., below the detection limit or below the rounding error in the calculation of the formula. All analyses were performed in cores.

Figure 2m (plane-polarized light) and Fig. 2n (cross-polarized light) are photographs of highly oxidized sample STR59.

Samples STR59 and STR903 (highly oxidized)

Petrographically, samples STR59 and STR903 are porphyritic. The main phenocrysts are euhedral to subhedral olivine, euhedral plagioclase, subhedral to anhedral clinopyroxene, anhedral Fe–Ti oxides, and anhedral apatite. In sample STR903 the olivine phenocrysts have a reaction rim of enstatitic orthopyroxene (Fig. 2f), whereas in STR59, orthopyroxene does not occur. The groundmass of these highly oxidized samples has a similar mineralogy, although olivine is notably absent whereas microlites of Fe–Ti oxides are ubiquitous (Fig. 2e).

In sample STR59 some of the olivine phenocrysts contain inclusions of clinopyroxene (Fig. 2h), which is described in detail below. In both samples, Fe–Ti oxides occur as inclusions within the olivine phenocrysts, often showing symplectitic intergrowth with olivine (Fig. 2i and j). Electron microprobe analyses of olivine

phenocrysts are given in Table 2. Olivine phenocrysts in the oxidized samples (STR59, STR903) are highly magnesian (Fo_{96–97}), whereas in typical Stromboli basalts (e.g. the control samples), they range from Fo₄₅ to Fo₈₃.

Clinopyroxene occurs in both STR59 and STR903 (Figs. 2f and 2g). Its composition lies within the field of diopsidic augite as in the normal Stromboli basalts (Fig. 3a), although the amount of ferric iron, calculated by charge balance, is higher than in the normal Stromboli clinopyroxene phenocrysts (Francalanci, 1993). Electron microprobe analyses of clinopyroxene phenocrysts are given in Table 3.

The orthopyroxene reaction rim on the olivine in sample STR903 contains a higher amount of ferric iron than normal (an ideal orthopyroxene should not contain ferric iron and ‘normal’ Stromboli samples typically contain <1 wt %). The Mg/Fe²⁺ ratio is comparable with that in the magnesium-rich olivine. Electron microprobe analyses of orthopyroxene phenocrysts are given in Table 3.

Fe–Ti oxides are anhedral, often forming symplectite-like intergrowths with olivine (Figs. 2i and 2j), or occur as

Table 3: Selected electron microprobe analyses of pyroxene phenocrysts (core, middle, rim) and groundmass (gm)

	STR47	STR4	STR86	STR281202c	SRT59	SRT59	SRT59	SRT59	SRT59	STR903	STR903	STR903	STR903	STR903
	core	core	core	core	rim	middle	core	core	gm	middle	rim	core	opx	opx
SiO ₂	51.31	48.80	50.85	48.37	50.29	50.61	50.64	51.70	50.03	51.16	50.08	51.03	57.28	56.55
TiO ₂	0.68	1.01	0.85	1.52	0.82	0.93	0.82	0.61	0.91	0.91	0.98	0.77	0.19	0.19
Al ₂ O ₃	1.93	4.62	2.74	5.21	3.17	3.11	2.62	2.14	3.41	3.25	3.50	3.02	1.66	2.01
Cr ₂ O ₃	0.02	0.13	0.07	0.05	0.07	0.09	n.a	0.03	n.a	0.04	0.13	0.03	n.a	0.01
Fe ₂ O ₃	2.22	4.70	2.83	3.36	4.39	2.22	3.25	3.70	5.08	0.87	4.71	2.87	n.a	1.70
FeO	7.46	3.85	5.81	5.98	2.45	7.13	5.77	3.66	1.79	7.60	2.67	4.76	3.82	2.39
MnO	0.24	0.18	0.31	0.33	0.32	0.28	0.26	0.29	0.40	0.24	0.34	0.22	0.73	0.77
MgO	15.51	13.82	14.80	13.36	16.05	14.33	14.96	15.92	16.58	13.90	14.99	14.55	34.76	35.17
CaO	20.00	22.90	21.63	21.41	21.96	20.99	21.30	21.30	21.17	21.64	22.10	21.90	1.46	1.30
Na ₂ O	0.23	0.28	0.29	0.36	0.45	0.33	0.31	0.63	0.61	0.36	0.59	0.59	0.05	0.06
Total	99.59	100.27	100.17	99.95	99.98	100.01	99.92	99.97	99.97	99.96	100.07	99.73	99.96	100.14
<i>Cations per 6 oxygens</i>														
Si	1.91	1.81	1.89	1.81	1.85	1.89	1.88	1.91	1.84	1.90	1.85	1.89	1.96	1.93
Ti	0.02	0.03	0.02	0.04	0.02	0.03	0.02	0.02	0.03	0.03	0.03	0.02	n.a	n.a.
Al	0.09	0.20	0.12	0.23	0.14	0.14	0.11	0.09	0.15	0.14	0.15	0.13	0.07	0.08
Cr	n.a	0.00	0.00	0.00	n.a	n.a	n.a	n.a	n.a	n.a	n.a	n.a	n.a	n.a.
Fe ³⁺	0.06	0.13	0.08	0.09	0.12	0.06	0.09	0.10	0.14	0.02	0.13	0.08	n.a	0.04
Fe ²⁺	0.23	0.12	0.18	0.19	0.08	0.22	0.18	0.11	0.06	0.24	0.08	0.15	0.11	0.07
Mn	0.01	0.01	0.01	0.01	0.01	0.01	0.01	0.01	0.01	0.01	0.01	0.01	0.02	0.02
Mg	0.86	0.77	0.82	0.74	0.88	0.80	0.83	0.88	0.91	0.77	0.83	0.80	1.78	1.79
Ca	0.79	0.91	0.86	0.86	0.87	0.84	0.85	0.84	0.83	0.86	0.87	0.87	0.05	0.05
Na	0.02	0.02	0.02	0.03	0.03	0.02	0.02	0.04	0.04	0.03	0.04	0.04	n.a	n.a.
total	3.99	4.00	4.00	4.00	4.01	4.00	4.00	4.00	4.01	4.00	4.00	4.00	4.00	4.00
<i>End-members (mol %)</i>														
jadeite	1.66	1.99	2.08	2.58	3.26	2.38	2.24	4.48	4.39	2.58	4.19	n.a	0.32	0.37
Fe ³⁺ CaTs	3.11	6.56	3.95	4.73	6.12	3.11	4.55	5.14	7.07	1.22	6.55	4.00	n.a	2.20
CrCaTs	0.04	0.19	0.11	0.07	0.11	0.14	n.a	0.04	n.a	0.06	0.18	0.04	n.a	0.01
TiCaTs	1.92	2.82	2.38	4.27	2.30	2.60	2.30	1.70	2.53	2.55	2.72	2.16	0.48	0.49
CaTs	1.49	6.31	2.57	5.91	2.99	3.03	2.33	0.71	2.70	3.28	2.80	2.31	2.72	2.07
woll	36.71	37.64	38.50	35.38	37.80	37.45	37.89	38.29	35.82	39.58	37.62	39.27	1.09	n.a.
en	43.14	38.26	40.93	37.23	44.28	39.79	41.51	43.78	45.74	38.54	41.29	40.24	88.84	90.30
fs	11.92	6.23	9.50	9.85	3.15	11.51	9.18	5.86	1.75	12.19	4.65	7.73	6.55	4.56

Analyses are in wt % and c.f.u. calculated on the basis of six oxygens in samples STR59 and STR903. Additional analyses are given from samples STR47, STR4, STR86 and STR281202c. n.a., below the detection limit, below the rounding in the calculation of the formula or below the error in the calculation of end-members. All analyses were performed in cores. End-members are from the method of Cawthorn & Collerson (1974). opx, orthopyroxene reaction rims on the Mg-rich olivine phenocryst. End-members: Fe³⁺CaTs, ferro-calcic Tschermak's end-member; TiCaTs, titanium-calcium Tschermak's end-member; CaTs, Ca-Tschermak's end-member; woll, wollastonite; En, enstatite; Fs, ferrosilite.

subhedral grain in the groundmass (Fig. 2e and f). For the 'normal' titanomagnetite in the control samples (Table 4) the ferric/ferrous iron ratio was calculated by charge balance (the trivalent cations must sum to two; total cations must sum to three). Applying the same procedure to the Fe-Ti oxides in samples STR59 and STR903 gives a perfect stoichiometry (cations sum to three) but the total is only 95 wt %. If we assume that all the iron is

in the ferric state, the total rises to 99–100 wt %. This suggests that the Fe-Ti oxides in both samples must actually be a solid solution between hematite and pseudobrookite. The Fe-Ti oxides thus reflect the same enrichment in Fe₂O₃ and FeO as the other ferro-magnesian phenocrysts (olivine, pyroxenes). Electron microprobe analyses of selected Fe-Ti oxides are given in Table 4.

Table 4: Selected electron microprobe analyses of Fe–Ti oxide phenocrysts

	STR47	STR4	STR86	STR86	STR-281202c	STR-281202c	STR-281202c	STR903	STR903
	gm	gm	gm	incl	gm	incl	incl	gm	gm
TiO ₂	8.71	17.48	6.32	0.09	3.63	0.49	0.37	8.93	10.42
Al ₂ O ₃	2.64	1.95	4.46	0.38	4.53	1.21	1.95	0.45	0.5
Cr ₂ O ₃	0.05	0.01	n.a.	0.04	0.00	0.00	0.01	n.a.	0.02
Fe ₂ O ₃	58.48	32.04	54.79	71.82	59.12	67.25	67.71	87.07	85.09
FeO	23.81	45.30	25.05	21.21	26.56	25.82	25.69	n.a.	n.a.
MnO	0.82	0.79	0.89	0.36	0.93	0.32	0.38	0.45	0.51
MgO	4.86	0.58	7.41	6.19	4.85	3.25	3.56	3	3.59
NiO	n.a.	0.01	0.03	0.10	0.07	0.04	0.07	0.03	0.02
ZnO	0.11	0.12	0.13	0.07	0.14	0.00	0.00	0.02	n.a.
Total	99.48	98.29	99.07	100.25	99.81	98.38	99.74	99.95	100.15

	STR903	STR903	STR903	STR903	STR59	STR59	STR59
	gm	gm	gm	incl	gm	incl	incl
TiO ₂	10.14	8.97	11.05	2.69	7.57	9.66	0.03
Al ₂ O ₃	0.43	0.46	0.45	1.27	1.53	1.5	n.a.
Cr ₂ O ₃	n.a.	n.a.	n.a.	n.a.	n.a.	0.01	0.01
Fe ₂ O ₃	86.03	87.28	83.35	93.65	86.54	84.07	100.07
FeO	n.a.	n.a.	n.a.	n.a.	n.a.	n.a.	n.a.
MnO	0.52	0.48	0.51	0.24	0.33	0.38	0.01
MgO	3.43	3.06	3.82	1.35	2.93	3.75	n.a.
NiO	n.a.	n.a.	0.03	0.04	0.01	n.a.	0.01
ZnO	0.04	0.04	0.03	n.a.	0.06	n.a.	n.a.
Total	100.59	100.29	99.24	99.23	98.97	99.37	100.13

Phenocrysts are in the control samples (STR47, STR4) sub-liquidus and sub-solidus oxidized samples (STR86, STR281202c) and highly oxidized samples (STR59, STR903). n.a., below the detection limit; gm, groundmass oxide; incl, oxide included in olivine. Ferric/ferrous iron in samples STR47, STR4 and STR281202c was calculated assuming that trivalent cations sum to two (titanomagnetite). Fe was assumed as ferric in STR59 and STR903.

Plagioclase exhibits a composition ranging from An₅₀ to An₇₀, within the normal range reported for Stromboli by Francalanci (1993), although some phenocrysts in STR59 have highly calcic cores of An₈₅, and some phenocrysts in sample STR903 exhibit a similar rim composition (An₈₀) (Fig. 3b). The normal zonation in sample STR59 and the inverse zonation in sample STR903 strongly suggest some degree of magma mixing, or, at least, heterogeneity in the composition of the melt. Electron microprobe analyses of plagioclase phenocryst are given in Table 5.

Samples STR281202c (sub-solidus oxidation) and STR86 (sub-liquidus oxidation)

Both samples are porphyritic and appear fresh and unoxidized in hand specimen (i.e. they are not reddened). The phenocrysts are olivine, clinopyroxene

and plagioclase. The groundmass is composed of Fe–Ti oxides, plagioclase and clinopyroxene; no olivine was found (Fig. 2a–d). The essential differences between these samples and those that are highly oxidized are: (1) the composition of the olivine phase: although the bulk-rock is oxidized in sample STR86 (Fig. 2a–d) the olivine has a normal composition; (2) the composition of the Fe–Ti oxides; (3) the textural differences between the symplectites found in the highly oxidized samples and these samples.

Olivine phenocrysts in samples STR281202c and STR86 have a composition of Fo_{82–85}, comparable with that of some of the typical Stromboli basalts (e.g. the control samples); this is slightly more forsteritic than olivine in the normal recent activity (Fo_{69–72}, Francalanci *et al.*, 2004). Electron microprobe analyses of representative olivine compositions in STR281202c and STR86 are given in Table 2.

Table 5: Selected electron microprobe analyses of feldspar phenocrysts

	STR47	STR4	STR86	STR281202c	STR59	STR59	STR59	STR59	STR59	STR903	STR903	STR903	STR903	STR903
	core	core	core	core	core	core	middle	middle	rim	middle	rim	rim	core	rim
SiO ₂	46.70	46.34	45.77	47.67	46.75	56.04	50.00	53.43	49.70	49.70	50.48	47.84	52.13	52.00
TiO ₂	0.06	0.01	0.06	0.00	0.05	0.09	0.03	0.10	0.07	0.00	0.04	0.04	0.09	0.13
Al ₂ O ₃	32.78	33.58	34.16	32.16	33.45	26.94	31.17	28.63	31.23	30.71	29.88	32.11	29.16	29.12
Fe ₂ O ₃	0.98	0.60	0.67	0.83	0.72	0.84	0.90	0.74	0.95	1.07	1.38	1.14	0.91	0.96
MnO	n.a.	0.00	0.00	0.00	n.a.	n.a.	n.a.	n.a.	n.a.	n.a.	n.a.	0.01	0.10	n.a.
MgO	n.a.	0.13	0.07	0.05	0.03	0.05	0.06	0.09	0.06	0.09	0.04	0.04	0.10	0.08
CaO	17.18	17.40	17.83	16.65	17.18	9.53	14.37	11.65	14.55	15.19	14.17	16.43	13.26	13.53
Na ₂ O	1.77	1.30	1.30	1.93	1.53	4.86	2.95	4.29	2.85	2.96	3.56	2.11	3.75	3.80
K ₂ O	0.20	0.23	0.17	0.21	0.21	1.74	0.49	1.09	0.50	0.28	0.31	0.20	0.55	0.37
Total	99.67	99.59	100.05	99.51	99.91	100.07	99.98	100.02	99.91	99.99	99.83	99.92	100.06	99.99
<i>Cations per 8 oxygens</i>														
Si	2.16	2.14	2.11	2.20	2.15	2.53	2.29	2.43	2.28	2.28	2.32	2.20	2.38	2.37
Al	1.79	1.83	1.86	1.75	1.82	1.44	1.68	1.53	1.69	1.66	1.62	1.74	1.57	1.57
Fe ³⁺	0.03	0.02	0.02	0.03	0.02	0.03	0.03	0.03	0.03	0.04	0.05	0.04	0.03	0.03
Mg	n.a.	0.01	0.01	n.a.	n.a.	n.a.	n.a.	0.01	n.a.	0.01	n.a.	n.a.	0.01	0.01
Ca	0.85	0.86	0.88	0.82	0.85	0.46	0.70	0.57	0.71	0.75	0.70	0.81	0.65	0.66
Na	0.16	0.12	0.12	0.17	0.14	0.43	0.26	0.38	0.25	0.26	0.32	0.19	0.33	0.34
K	0.01	0.01	0.01	0.01	0.01	0.10	0.03	0.06	0.03	0.02	0.02	0.01	0.03	0.02
Total	5.00	5.00	5.01	5.00	5.00	4.99	5.00	5.01	5.00	5.01	5.02	5.00	5.00	5.00
<i>Mol % end-members</i>														
An	83.33	87.01	87.51	81.71	85.13	46.90	70.94	56.53	71.75	72.94	67.64	80.26	64.45	65.08
Ab	15.69	11.64	11.49	17.10	13.65	42.96	26.20	37.24	25.33	25.48	30.61	18.57	32.41	32.80
Or	0.98	1.33	0.97	1.19	1.22	10.14	2.87	6.23	2.92	1.58	1.75	1.16	3.14	2.12

Analyses are in wt % and c.f.u. recalculated on the basis of eight oxygens in samples STR59 and STR903. An additional analysis is given from sample STR47 for comparison. n.a., below the detection limit, or below the rounding in the calculation of the formula. All analyses were performed in cores.

Clinopyroxene occurs in both STR281202c and STR86 (Fig. 2a and c). The phenocrysts are strongly zoned in STR86, but are more homogeneous in STR281202c. The composition in sample STR86 varies within the field of diopsidic augite to salite, whereas compositions in STR281202c are constrained mainly in the augite field (Fig. 3a). Electron microprobe analyses of representative clinopyroxene phenocrysts in both samples are given in Table 3. As will be shown below, the differences in the composition of the clinopyroxene phase in the groundmass allow us to distinguish between sub-liquidus and sub-solidus oxidation in these samples.

Fe–Ti oxides occur in veins or cracks in the olivine phenocrysts, often intergrown with pyroxene, or as sub-hedral grains in the groundmass (Fig. 2a–d). The composition of the inclusions in the olivine phenocrysts in sample STR281202c varies from $X_{ulv} = 0.01$ to 0.09. Those in the olivine phenocrysts in sample STR86 could not be analysed because of their small size. Groundmass

Fe–Ti oxides in sample STR86 are normal titanomagnetites similar to those in the other control samples. Electron microprobe analyses of selected Fe–Ti oxides phenocrysts are given in Table 4.

Plagioclase varies in composition from An₆₀ to An₉₀, similar to that in the highly oxidized samples and the normal range reported for Stromboli by Francalanci (1993; Fig. 3b). Electron microprobe analyses of plagioclase phenocrysts are given in Table 5.

BULK-ROCK CHEMISTRY

Major element geochemistry

Detailed discussions of the bulk-rock chemistry of the Stromboli lavas have been published previously by Francalanci *et al.* (1989, 1993, 2004) and Hornig-Kjarsgaard *et al.* (1993). In Table 6 we report only the major and trace element analyses of the two highly oxidized samples (STR59, STR903), together with data

Table 6: Bulk-rock major, trace and REE chemical analyses

Period: Sample:	Control		Sub-liquidus oxidation	Sub-solidus oxidation	Highly oxidized	
	Lower Vancori STR47	Neostromboli STR4	Neostromboli STR86	Recent STR281202c	Neostromboli STR59	Recent STR903
SiO ₂	51.28	51.93	52.64	49.80	53.39	50.53
TiO ₂	0.9	0.9	0.92	0.98	0.84	1.03
Al ₂ O ₃	18.18	17.45	16.37	18.15	17.61	17.43
Fe ₂ O ₃	1.77	1.26	3.99	5.37	6.82	7.75
FeO	6.35	6.03	3.8	3.15	0.63	0.75
MnO	0.16	0.14	0.15	0.16	0.14	0.15
MgO	5.64	5.93	5.47	6.48	4.64	6.09
CaO	10.28	8.76	9.25	10.60	8.6	10.1
Na ₂ O	2.36	2.18	2.5	2.51	2.78	2.4
K ₂ O	2.12	4.63	3.57	2.19	3.43	2.61
P ₂ O ₅	0.37	0.5	0.5	0.40	0.41	0.57
LOI	0.52	0.23	0.8	0.21	0.64	0.58
Total	99.93	99.94	99.96	100.00	99.93	99.99
Rb	71	152	125	71.0	124	65
Sr	657	773	685	744.3	651	734
Ba	739	1782	1486	929.5	1258	955
Zr	139	188	198	144	203	150
Nb	15.86	28	24	21.7	25.25	21.54
V	270	n.d.	n.d.	261.5	224	260
Y	26.07	27	n.d.	27.4	28.03	25.34
La	33.5	56	n.d.	46.5	47.13	44.99
Ce	64	99	104	103.4	93	91
Nd	32.05	45	n.d.	46.0	41.46	41.72
Sm	6.4	10.8	n.d.	9.1	8.17	8.13
Eu	1.62	2.2	n.d.	2.4	2.03	2.13
Tb	0.8	0.95	n.d.	1.1	0.94	0.93
Yb	2.09	2.2	n.d.	2.6	2.4	2.19
Lu	0.35	0.5	n.d.	0.4	0.36	0.33
Th	12.53	18.1	n.d.	16.5	18.48	10.75
Ta	0.84	1.2	n.d.	1.6	1.22	1.11
Hf	3.26	4.2	n.d.	4.0	4.41	3.33
Cr	34.8	140	n.d.	47.1	75.5	52.8
Sc	31.6	28	n.d.	30.0	n.a.	n.a.
Co	32.2	30	n.d.	34.7	27.7	32.3
Ni	41.3	34	46.0	35.0	37.7	42.8

Analyses are of samples STR47, STR4 (control samples), STR86, STR281202c (sub-liquidus and sub-solidus oxidation), and STR59 and STR903 (highly oxidized) (see text for analytical details). Trace elements and REE were analysed in this study. n.d., data are not available.

for the control samples STR47 from the Lower Vancori period and STR4 from the Neostromboli period, the sub-liquidus oxidized sample STR86 (Neostromboli) and the sub-solidus oxidized sample STR281202c (Recent). The range of variation of wt % K₂O vs wt % SiO₂ for these

samples is shown in Fig. 4a, and Fe₂O₃/FeO weight ratio vs wt % SiO₂ in Fig. 4b. In both diagrams fields for the Vancori and Recent, Neostromboli and Paleostromboli sequences from the background database are shown for comparison. On the basis of the K₂O vs SiO₂ diagram

the samples are, consistent with their petrographic characteristics, basalts and basaltic andesites. The samples with magnesium-rich olivine (STR59, STR903) do not differ significantly from the control samples in terms of their major element chemistry. The eruptives of the Neostromboli period, including STR59 from the transition between the Upper Vancori and Neostromboli periods, have a characteristic potassium-rich, leucite-normative shoshonitic, chemistry (Fig. 4a), which has been previously discussed by Francalanci *et al.* (1989). The ejected lithic block STR903 also has a shoshonitic chemistry comparable with the basalts of the Vancori period and the recent phase of activity [the geochemical similarity between the basalts of both periods has been pointed out by previously by Francalanci *et al.* (1989, 1993)]. STR903 has a different, less potassic and more primitive magma composition than STR59. This has an important implication: independent of the age of STR903, the

unusual process that produced the magnesium-rich olivine must have happened more than once in the history of the volcano.

From the $\text{Fe}_2\text{O}_3/\text{FeO}$ weight ratio vs wt % SiO_2 diagram (Fig. 4b), it is evident that this ratio is not significantly affected by shallow-level differentiation processes, remaining between 0.5 and one for most of the Stromboli samples. The variance is larger in the Vancori and the Neostromboli periods than in the Recent and Paleostromboli periods (Table 7). The most characteristic feature of the samples with the magnesium-rich olivine phenocrysts (STR903 and STR59) is their high Fe_2O_3 content (and $\text{Fe}_2\text{O}_3/\text{FeO}$ ratio) in comparison with the control (STR47, STR4), the sub-liquidus oxidized (STR86) and the sub-solidus oxidized samples (STR281202c), and the background dataset.

The oxidation state of iron in the samples, as previously mentioned, was independently measured by wet

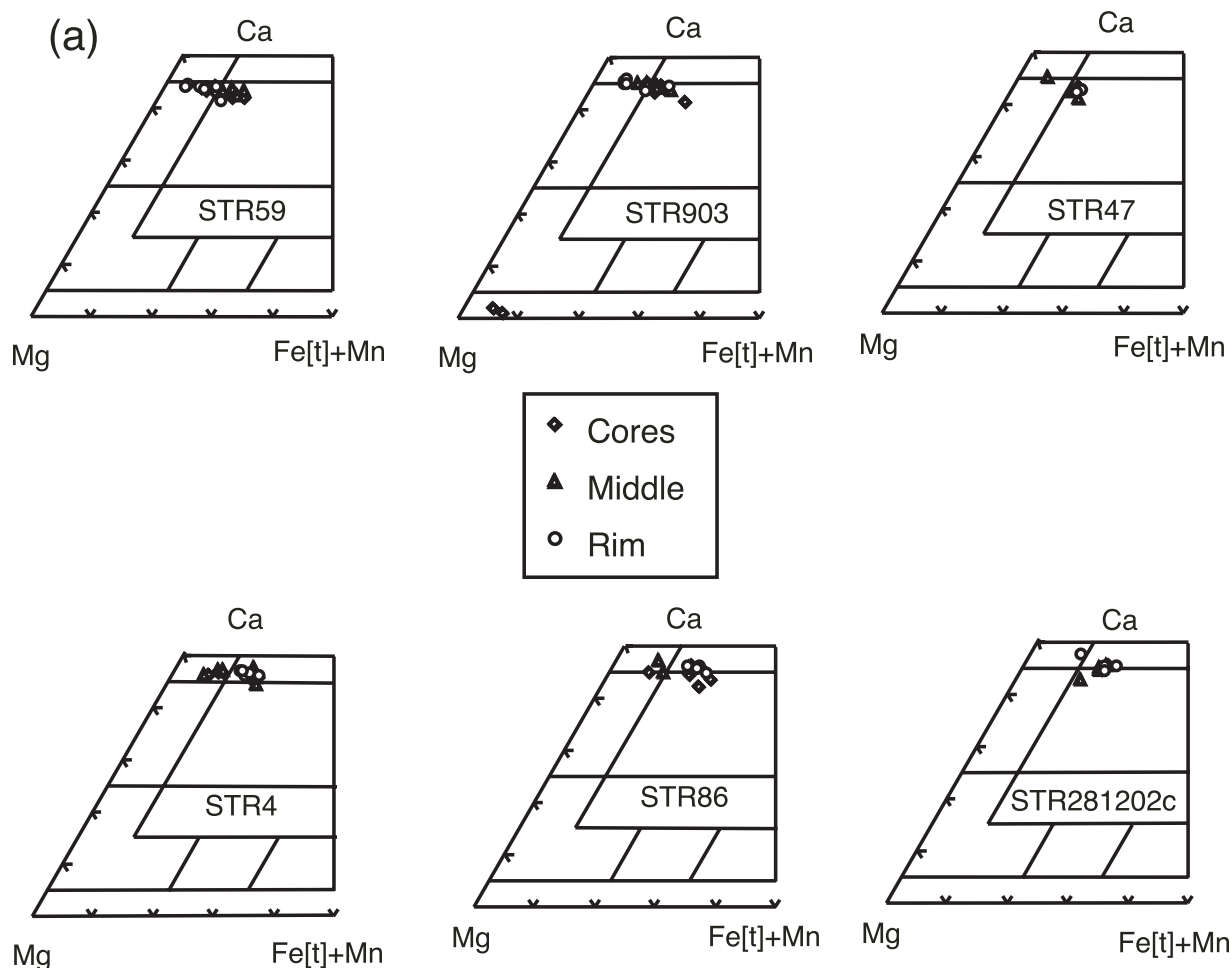


Fig. 3. (a) Wollastonite (Ca)–enstatite (Mg)–ferrosilite (Fe[t] + Mn) classification diagram for pyroxene phenocrysts in samples STR59, STR903, STR47, STR4, STR86 and STR281202c. Fe(t) includes ferric and ferrous iron and manganese. Classification fields are from Deer *et al.* (1997b). (b) Anorthite (Ca)–albite (Na)–orthoclase (K) classification diagram for plagioclase phenocrysts in samples STR59, STR903, STR47, STR4, STR86 and STR281202c.

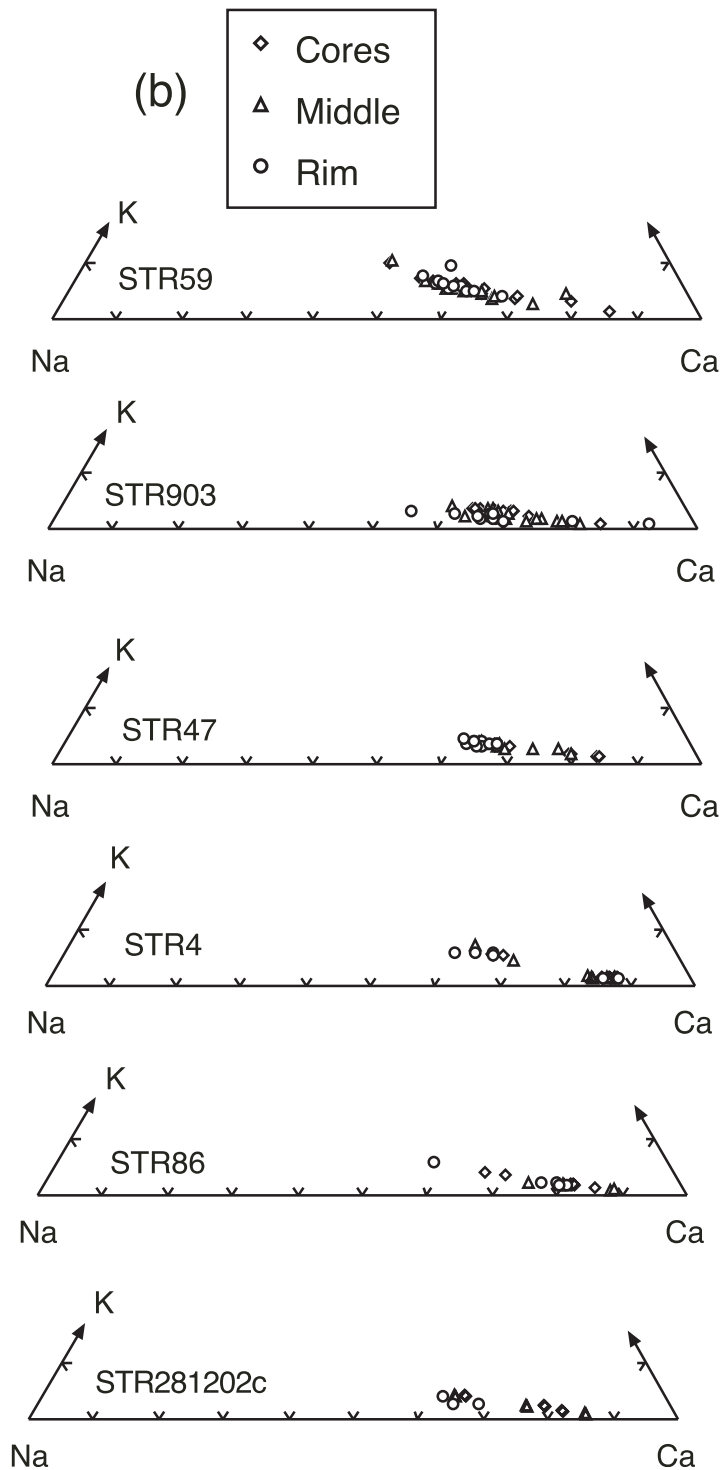


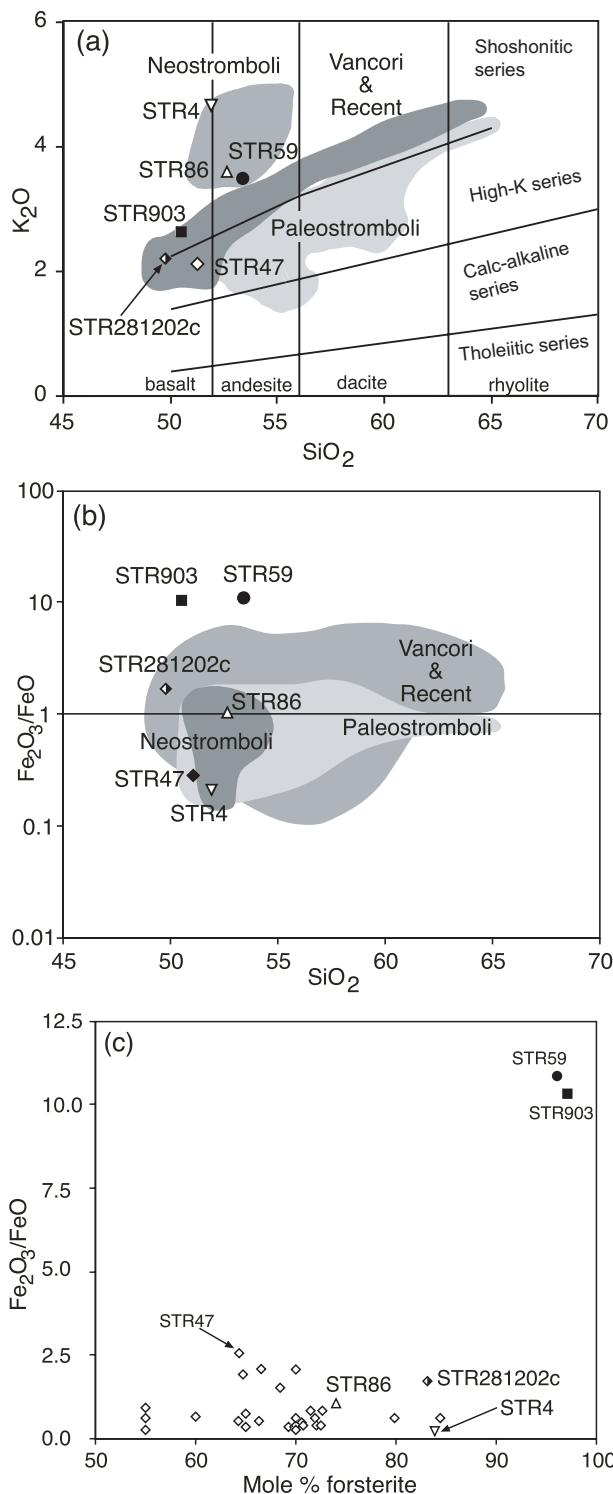
Fig. 3. Continued

chemical methods, and not estimated from the XRF results; hence, these data are not an analytical artefact. Within the dataset there are some samples with up to three times higher $\text{Fe}_2\text{O}_3/\text{FeO}$ weight ratios in the

bulk-rock chemical composition than average; however, the two samples with magnesium-rich olivine phenocrysts (STR903 and STR59) have 10 times more Fe_2O_3 than FeO (on a wt % basis). This highly oxidized state of iron

appears to be a primary characteristic of these particular samples, as the loss on ignition of the samples is low (<1 wt %) and, from the point of view of the mineralogy and mineral chemistry, the samples are petrographically

unaltered. Additional evidence for high wt % Fe_2O_3 being a primary feature of the magma chemistry is the higher ratio of $\text{Fe}^{3+}/\text{Fe}^{2+}$ in the clinopyroxene phenocrysts in these samples compared with those in the normal Stromboli samples; this is discussed in detail below.



Relationship between bulk-rock $\text{Fe}_2\text{O}_3/\text{FeO}$ and olivine composition

Olivine phenocryst compositions (mole % forsterite) are plotted in Fig. 4c versus the $\text{Fe}_2\text{O}_3/\text{FeO}$ weight ratio in the bulk-rocks for the samples from this study and additional samples from Francalanci *et al.* (2004) and Cortés *et al.* (2005). It is evident that the olivine composition is independent of the $\text{Fe}_2\text{O}_3/\text{FeO}$ weight ratio for values of the ratio below 1.0, and for forsterite contents below 85 mole %. The highly forsteritic olivine phenocrysts are distinct, suggesting that if there is any functional relationship between the two parameters, it must be strongly hyperbolic.

Trace elements

Primitive mantle-normalized trace element patterns, normalized according to the data of McDonough & Sun (1995), for the high $\text{Fe}_2\text{O}_3/\text{FeO}$ weight ratio samples (STR903, STR59) and the control samples STR47 and STR4 (as representatives of the High-K and shoshonitic series) are shown in Fig. 5. From these diagrams, it is evident that the different oxidation state of the 'normal' and 'oxidized' samples is not reflected in their trace element characteristics. Similarly, there is no difference between the sub-liquidus (STR86) and sub-solidus (STR281202c) oxidized samples and the other samples.

DISCUSSION

As mentioned previously, the highly oxidized samples STR59 and STR903 represent the crystallization products of two different magma compositions that were erupted at different geological times. This has important

Fig. 4. (a) K_2O vs SiO_2 (wt %) classification diagram, according to Peccerillo & Taylor (1976), for highly oxidized samples STR59, STR903 (filled symbols), control samples STR4, STR47, sub-liquidus oxidized sample STR86 and sub-solidus oxidized sample STR281202c (open or half-filled symbols). The background dataset for Stromboli lavas is from Francalanci *et al.* (1989, 1993) and Hornig-Kjarsgaard *et al.* (1993), and is used to define fields (shaded) for the Vancori & Recent, Neostromboli and Paleostromboli periods. (b) $\text{Fe}_2\text{O}_3/\text{FeO}$ wt % ratio vs wt % SiO_2 for the highly oxidized and control samples and the main volcanic periods as in (a). All the symbols and shadings are as in (a). (Note that the vertical axis is on a log₁₀ scale.) (c) Mole % forsterite in olivine phenocrysts vs bulk-rock $\text{Fe}_2\text{O}_3/\text{FeO}$ wt % ratio in samples STR4, STR86, STR47, STR281202c, STR59 and STR903. Additional data for normal Stromboli basalts are from Francalanci *et al.* (2004).

Table 7: Mean (\bar{X}), standard deviation (σ_{n-1}) and number of samples (n) of the calculated (Fe_2O_3/FeO) weight ratio from bulk-rock chemical analyses

Unit	\bar{X}	σ_{n-1}	n
PS I	0.72	0.31	41
PS II	0.62	0.70	32
PS III	0.86	0.42	40
Vancori	1.27	1.82	80
Neostromboli	0.84	1.72	55
Recent	0.55	0.22	21

Bulk-rock chemical analyses are from Francalanci (1993) Francalanci *et al.* (1993) and Hornig-Kjarsgaard *et al.* (1993). PS I, Paleostromboli I; PS II, Paleostromboli II; PS III, Paleostromboli III.

implications; the fact that the oxidation process has occurred at least twice suggests a fundamental cause rather than a statistical anomaly. In the following section we will attempt to constrain this process.

First it is important to identify the conditions of the magmatic system when STR59 and STR903 were erupted; possible scenarios by which to form olivine with >92 mole % forsterite in basalt–basaltic andesite magmas need to be established. The alternatives are as follows.

(1) The olivine has a metamorphic origin, resulting from a two-stage process in which less magnesium-rich olivine is altered to serpentine (losing iron, as magnetite, and gaining water), and then subsequently is reheated, losing the water and becoming a more magnesium-rich olivine. This process has been proposed previously by Trommsdorff & Evans (1972) to form magnesium-rich olivine in meta-serpentinites, and was subsequently invoked by Trommsdorff & Evans (1974) and Trommsdorff *et al.* (1998) to explain the transport of water within the mantle wedge above subduction zones. Haggerty & Baker (1967) performed an early experimental study to simulate this process. Along the same line of reasoning forsteritic olivine can also be produced by the metamorphism of dolomitic limestone in a skarn-type reaction. This is, however, a most unlikely scenario, as there is no evidence for the existence of limestone in the crust under Stromboli (Ferrari & Manetti, 1993) and carbonate-rich xenoliths have not been found in Stromboli lavas (Honnorez & Keller, 1968; Renzulli *et al.*, 2001; Renzulli *et al.*, 2003).

(2) The composition of the olivine is the original composition at the time of crystallization. To achieve this the amount of Fe^{2+} in the melt must have been significantly depleted and, therefore, not available to enter the olivine structure. This would require olivine crystallization from

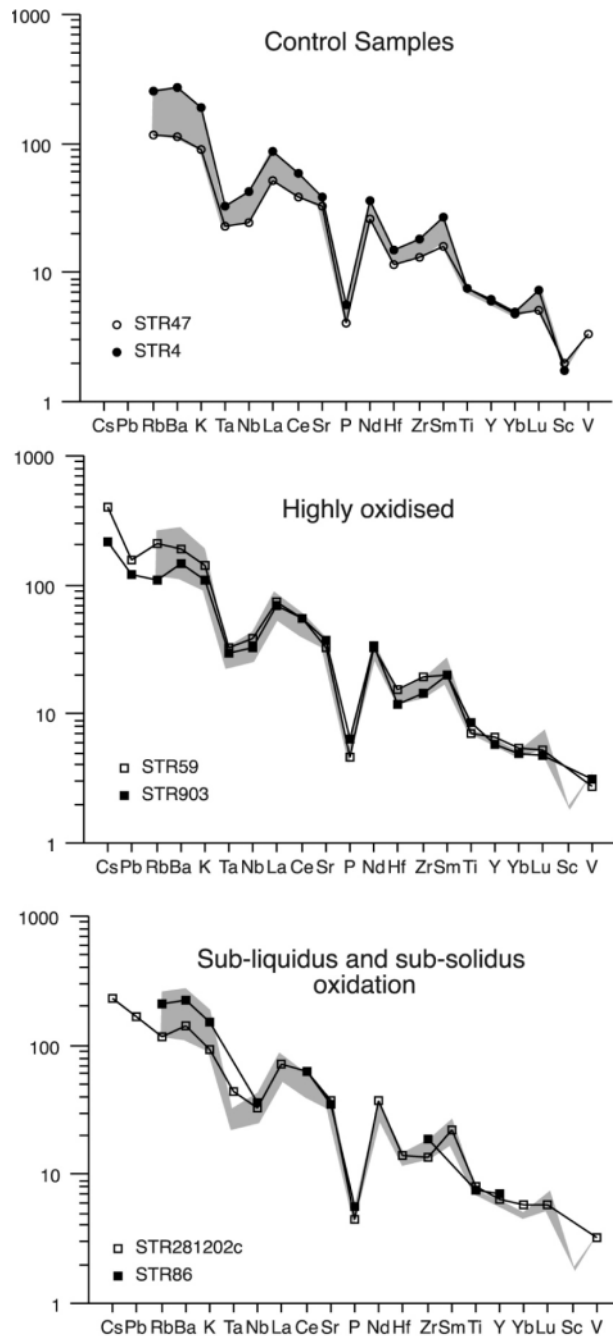


Fig. 5. Primitive mantle normalized trace element variation diagrams for the highly oxidized samples STR59, STR903, sub-liquidus oxidized sample STR86, sub-solidus oxidized sample STR281202c, and the control samples STR47 and STR4. Normalization constants are from McDonough & Sun (1995). The shaded field in (a)–(c) is defined by the control samples.

a highly oxidized magma with most of the iron in the ferric state. A similar process was proposed by Wager & Brown (1967) to explain the compositions of cumulus olivine phenocrysts in the Skaergaard intrusion,

Greenland, although in this case the composition of the olivine phenocrysts was in the normal range. Subsequently, an occurrence of almost pure forsterite olivine phenocrysts (Fo_{98.5}) was reported by Sigurdsson & Brown (1970) from a tholeiitic basalt from the Kolbeinsey Ridge on the extension of the Mid-Atlantic Ridge between Iceland and Jan Mayen. Those workers attributed the magnesium-rich composition of the olivine to the unusual oxidation state of the magma, at the time of crystallization, caused by interaction with seawater.

On the basis of the symplectitic intergrowth between the forsteritic olivine and Fe–Ti oxides in the highly oxidized samples (Fig. 2i and j) it might be argued that this texture is a sub-solidus feature, favouring alternative (1). However, there are significant differences in the textures of the olivine and Fe–Ti oxide intergrowths in samples STR59 and STR903 compared with those produced experimentally by Haggerty & Baker (1967) or those, shown in Fig. 2a–d, from the sub-liquidus (STR86) or sub-solidus (STR281202c) oxidized samples. In particular, the symplectites described by Haggerty & Baker (1967) are either oriented or radial, or occur as reaction rims, whereas in samples STR59 and STR903, pseudobrookite tends to grow pervasively and without preferred orientation (Fig. 2i and j). The presence of pseudobrookite in the symplectites in STR59 and STR903 is also significant. Metamorphic breakdown of a normal olivine phenocryst cannot produce a Ti-rich oxide because Ti is present only as a trace element in olivine. Furthermore, the textures shown in Fig. 2e–j do not resemble those of metamorphosed olivine phenocrysts (B. W. D. Yardley, personal communication, 2004) and are very similar to those described by Sigurdsson & Brown (1970).

On the basis of the above we consider that there is compelling evidence that the Mg-rich olivine phenocrysts are primary, and that they were formed under highly oxidizing conditions. Both highly oxidized samples were erupted in association with paroxysmic activity, linked with partial or total collapse of the volcanic edifice. Sample STR281202c, which also shows evidence of oxidation, was collected at the beginning of the 2002–2003 volcanic crisis. However, we consider that the process of oxidation in the case of STR281202c is not primary but occurred sub-solidus after the olivine phenocrysts had already crystallized, causing a metamorphic-like breakdown of the normal olivine phase into magnetite + orthopyroxene.

Equilibrium between forsteritic olivine and the host melt

To evaluate if the forsteritic olivines were in equilibrium with their host magma we calculated the olivine–melt partition coefficient, following Roeder & Emslie (1970),

assuming that the bulk-rock chemistry of the samples can be used as a proxy for the composition of the original melt; the resultant $K_D(\text{ol}/\text{melt})$ is 0.39. As pointed out by Carmichael & Ghiorso (1990), the olivine–melt partition coefficient has a mean value of 0.34, ranging between 0.3 and 0.4. This is valid for melts that cover a range of compositions between 41.9 and 66.6 wt % SiO₂ and olivine compositions from Fo₉₈ to Fo₅₂, liquidus temperatures from 1064 to 1400°C, and log $f\text{O}_2$ values between –0.68 and –14.1. We can, therefore, be confident that the magnesium-rich olivine crystallized in equilibrium with a melt in which the MgO/FeO weight ratio was similar to that of the bulk-rock chemical analysis, and, therefore, that this Mg-rich phase was in equilibrium with the host magma.

Estimation of oxygen fugacity in the Stromboli basalts

The estimation of oxygen fugacity in magmas is usually based on mineral equilibria involving, for example, the equilibrium between magnetite and ilmenite, as calibrated by Sack & Ghiorso (1991) among others. However, the only Fe–Ti oxide found in samples STR59 and STR903 is close to a pseudobrookite–hematite solid solution in composition, and, therefore, it is not possible to apply the usual free energy considerations in this scenario. Additionally, titanomagnetite is the only Fe–Ti oxide present in the normal Stromboli products (Francalanci, 1993). Another possibility is to use the empirical relationship between Fe₂O₃/FeO (molar ratio) in the melt and oxygen fugacity ($f\text{O}_2$), determined by linear regression of experimental data for basaltic glasses [equation (1)], originally by Sack *et al.* (1980), and subsequently refined by Kilinc *et al.* (1983) and Kress & Carmichael (1988):

$$\ln\left(\frac{x_{\text{Fe}_2\text{O}_3}}{x_{\text{FeO}}}\right) = a \ln f\text{O}_2 + \frac{b}{T} + c + \sum_i d_i x_i \quad (1)$$

where a , b , c , and d_i are experimental parameters ($i = \text{Al}_2\text{O}_3, \text{FeO}^*, \text{CaO}, \text{Na}_2\text{O}, \text{K}_2\text{O}$), x_i are mole fractions, and T is the temperature in Kelvin (see Table 8).

Kilinc *et al.* (1983) calibrated equation (1) for highly oxidizing conditions (in equilibrium with the atmosphere, or equivalent, with log $f\text{O}_2 = -0.678$), demonstrating that under such conditions a basaltic magma can crystallize olivine as MgO-rich as Fo₉₈, whereas the same magma equilibrated under the more reducing conditions of the quartz–fayalite–magnetite (QFM) oxygen buffer would crystallize Fo₈₃. Sugawara (2001) also reached similar conclusions (crystallization of Fo₉₇, with log $f\text{O}_2 = -0.68$).

Although our samples are clearly not glasses, we have assumed that they crystallized from a basaltic melt

Table 8: Regression coefficients for equation (1) [from Kilinc *et al.* (1983)], with one standard error

Parameter	Value	Standard error
<i>a</i>	0.2185	0.0044
<i>b</i>	12670	900
<i>c</i>	-7.54	0.55
$d_{\text{Al}_2\text{O}_3}$	-2.24	1.03
d_{FeO^*}	1.55	1.03
d_{CaO}	2.96	0.53
$d_{\text{Na}_2\text{O}}$	8.42	1.41
$d_{\text{K}_2\text{O}}$	9.59	1.45

geochemically similar to the bulk-rock composition, and we have used the Kilinc *et al.* (1983) relationship to provide some constraints on the order of magnitude of the oxygen fugacity. Given that some samples from our dataset might have secondary oxidized groundmasses, the results obtained clearly represent only a maximum value for the oxygen fugacity. Such secondary oxidation might be responsible for the relatively high variance in $\text{Fe}_2\text{O}_3/\text{FeO}$ in some of the volcanic periods shown in Fig. 4b. Equation (1), calibrated with the parameters of Kilinc *et al.* (1983) (Table 8), was applied to both the oxidized and the control samples. Temperatures were calculated using olivine–clinopyroxene pairs in the control samples using the method of Loucks (1996). A temperature of 1033°C was assumed in the oxidized samples (estimated to be the same as sample STR281202c) because the method of Loucks (1996) cannot be applied under high oxygen fugacity conditions (Table 9). This gives a $\log f\text{O}_2$ of -1.2 for sample STR59 and -1.1 for sample STR903. These values are equivalent to a ΔQFM of ≈ 9 relative to the QFM oxygen buffer experimental fit of O'Neill (1987). In practical terms, we can assume with confidence a value of oxygen fugacity equivalent to that in equilibrium with air ($10^{-0.678}$ bar, $\Delta\text{QFM} = +8.7$), as for natural systems this must be considered the upper limit of the oxidation state. The calculated oxygen fugacity of the oxidized and the control samples, together with the oxygen fugacity curves for the QFM and HM (hematite–magnetite) oxygen buffers, are indicated in Fig. 6.

To find a more explicit relation between the bulk-rock $\text{Fe}_2\text{O}_3/\text{FeO}$ weight ratio and the intrinsic oxygen fugacity, the Kilinc *et al.* (1983) equation (1) was applied to the entire dataset of Francalanci *et al.* (1989, 1993, 2004) and Hornig-Kjarsgaard *et al.* (1993). To calculate the numerical value of the oxygen fugacity, three temperatures were used within the normal magmatic range (1000°C, 1100°C and 1200°C). ΔQFM was then

Table 9: Calculated temperatures in the control samples using olivine–clinopyroxene pairs and the method proposed by Loucks (1996), and oxygen fugacity

Sample	$T(^{\circ}\text{C})$	<i>n</i>	σ_{n-1}	$f\text{O}_2$ (bars)	ΔQFM
STR86	1053	19	173	-5.59	4.73
STR4	969	6	120	-10.13	1.46
STR47	1090	9	30	-7.33	2.47
STR281202c	1033	11	178	-4.62	5.99
STR59	n.a.	n.a.	n.a.	-1.18	9.42
STR903	n.a.	n.a.	n.a.	-1.10	9.50

Calculated oxygen fugacity was determined using the method of Kilinc *et al.* (1993). n.a., not calculated (see text for details); $T(^{\circ}\text{C})$, temperature in degrees Celsius; *n*, number of calculations per sample; σ_{n-1} , standard deviation of the calculation; $f\text{O}_2$, absolute oxygen fugacity; ΔQFM , oxygen fugacity related to the QFM buffer of O'Neill (1987).

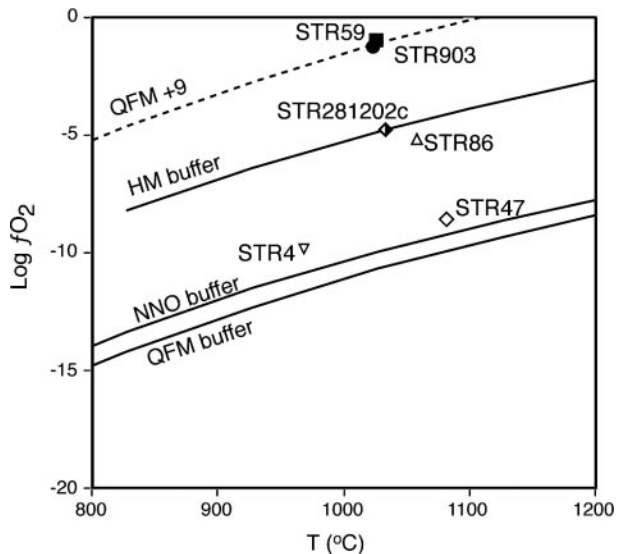


Fig. 6. $\log f\text{O}_2$ vs temperature for the highly oxidized samples STR59, STR903, sub-liquidus oxidized sample STR86, sub-solidus oxidized sample STR281202c, and the control samples STR47 and STR4. QFM buffer curve is from O'Neill (1987); NNO curve is from Huebner & Sato (1970); HM buffer curve is from Myers & Eugster (1983). Dashed line represents QFM + 9. Symbols are as in Fig. 4a.

calculated using the experimental fit of O'Neill (1987) at the same temperatures. We find that: (1) only the $\text{Fe}_2\text{O}_3/\text{FeO}$ weight ratio in the bulk-rock has a significant effect on the calculation of the oxygen fugacity; variation in the proportion of alkalis has a minor effect on the results and can be neglected (note that the dataset contains samples from the calc-alkaline, High-K and shoshonitic magma series); (2) the calculated value of ΔQFM is essentially independent of temperature.

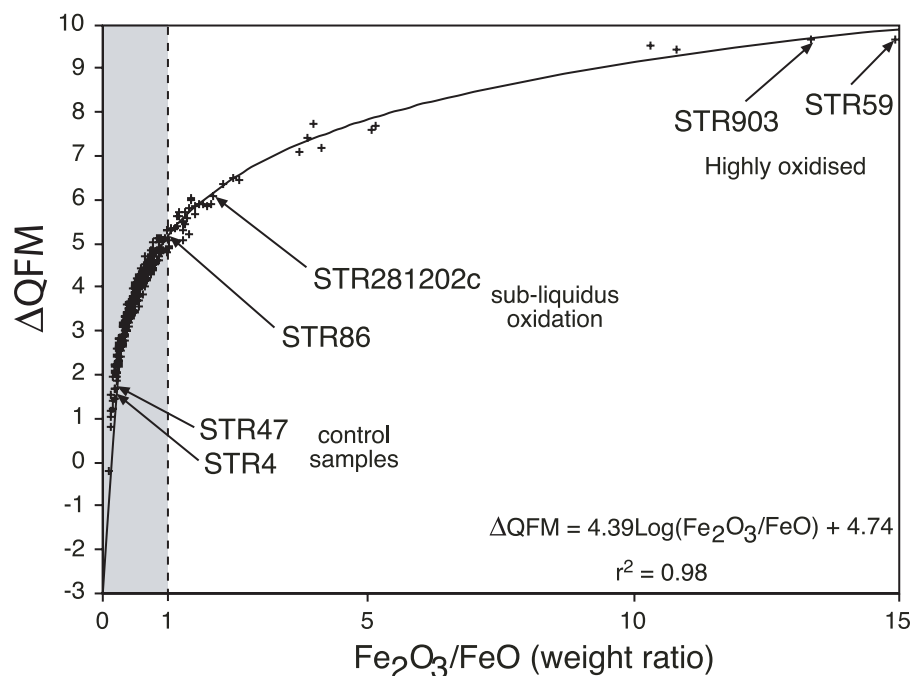


Fig. 7. ΔQFM vs $\text{Fe}_2\text{O}_3/\text{FeO}$ weight ratio in the bulk-rocks, calculated using the approach of Kilinc *et al.* (1983) and the experimental QFM buffer curve of O'Neill (1987) for samples from the dataset of Francalanci *et al.* (1989, 1993, 2004) and Hornig-Kjarsgaard *et al.* (1993). The samples from the present study are highlighted.

In Fig. 7 we show the results of the calculation for 290 samples from the dataset. A logarithmic fit to the data is shown with $r^2 = 0.98$, showing an excellent correlation between the $\text{Fe}_2\text{O}_3/\text{FeO}$ weight ratio in the samples and oxygen fugacity reported as ΔQFM . The upper boundary of the shaded area represents an $\text{Fe}_2\text{O}_3/\text{FeO}$ weight ratio equal to one, which is equivalent to $\Delta\text{QFM} = 4.74$. Consistently, the gap already observed in the olivine phenocryst compositions is also present in the relation between the $\text{Fe}_2\text{O}_3/\text{FeO}$ weight ratio and the intrinsic oxygen fugacity.

The oxidation process

Having established that the oxidation process takes place in association with major paroxysmic events, producing anomalous Mg-rich olivine phenocrysts, we now need to constrain under what conditions such oxidation can occur. As pointed out by Carmichael (1991), the oxidation state of magmas is principally related to that of their mantle source regions, unless the ascending magmas are open to oxygen. Therefore, it is clear that the Stromboli magmas must have become oxidized at some point after they were generated in the mantle wedge above the Aeolian subduction zone. In this scenario, the candidate oxidizing agents are: (1) the equilibrium of the melt with the atmosphere; (2) the addition of water to the melt; (3) the exsolution and dissociation of water already dissolved in the melt; or (4) the exsolution and

degassing of other fluid phases such as sulphur and carbon compounds.

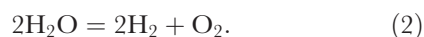
The interface with the atmosphere

The contact of a basaltic melt with the atmosphere seems to be the most likely natural process to cause extreme oxidation, as suggested by the experimental results of Kilinc *et al.* (1983) and Sugawara (2001) among others. Indeed, Stromboli has an active lava lake, and so by definition is an open system in contact with the atmosphere. An inspection of the composition of the normal eruptive products, however, shows that the oxidation state does not depart significantly from 2 log units above the QFM buffer (samples STR47 and STR4; Fig. 6). Therefore, this is an unlikely process to explain the extreme oxidation in samples STR59 and STR903. Additionally, there is an essential difference between the equilibrium experiments producing Mg-rich olivine phenocrysts and volcanic systems with an active lava lake. The key factor lies in the conditions of the experiments, which are closed systems and reach equilibrium. In contrast, an active lava lake is by definition an open system, and although it can reach steady state, it can never reach equilibrium because of the continuous input of new magma/volatiles and persistent degassing. Therefore, we conclude that this process is not the cause of the extreme oxidation of some Stromboli magmas.

Role of water

Another process by which highly oxidizing conditions might be created, postulated by Sigurdsson & Brown (1970) to explain the occurrence of Mg-rich olivines in the Kolbeinsey basalt, is the interaction of magma with water. It has been demonstrated that dissolving water in silicate melts has little (Baker & Rutherford, 1996), or no (Moore *et al.*, 1995; Gaillard *et al.*, 2001) effect on the ferric–ferrous ratio of silicic melts; there might, however, be an effect on more mafic magmas. We shall demonstrate that, potentially, a typical Stromboli basalt has enough dissolved water eventually to produce a high level of oxidation, without the need to involve an external source of water. Additionally, if water is the agent that induces the oxidation process, we should expect to find more examples of highly oxidizing conditions in natural magmas, whereas in fact most occurrences of water–lava interaction produce quenched textures and normal oxidation states.

Assuming that free oxygen is produced only by the dissociation of molecular water present in the melt, we can estimate the amount needed to oxidize the melt to $\Delta\text{QFM} = +8.7$. First, assuming that oxygen fugacity is equal to the oxygen partial pressure in the melt (or equivalently, that oxygen behaves as an ideal gas), we can use the ideal gas equation to estimate the number of moles of oxygen equivalent to such a partial pressure. At a partial pressure of oxygen equivalent to $10^{-0.678}$ bars and a temperature of 1306 K (= 1033°C) there are 1.94 moles of free oxygen per m^3 of magma. If we suppose that all the free oxygen was produced from the dissociation of water (we can neglect the partial pressure of oxygen at QFM buffer conditions), 3.88 moles of water per m^3 of magma are needed to produce the amount of oxygen required by the dissociation reaction



This amount of water is equivalent to 69.84 g of H_2O per m^3 . Assuming a density of basaltic magma of $2.7 \times 10^6 \text{ g/m}^3$, we can estimate that the dissociation of 0.026 wt % water is sufficient to produce the amount of oxygen required. According to Stolper (1982), <1 wt % of dissolved water, within the normal range of water contents in basalts, in the melt is required to have 0.2 wt % of molecular water potentially available for dissociation. This result has two important implications. First, there is no need for an additional source of water to produce the amount of oxygen required, as there is already enough in the melt. Second, because the normal Stromboli basalts usually have >2 wt % water (Francalanci *et al.*, 1989, 1993) and most of the basalts have oxidation states between the QFM and the nickel–nickel oxide (NNO) buffers, it follows that

dissolved water in magmas on its own is unlikely to produce the high degree of oxidation in STR59 and STR903. Here again a key point is the difference between the natural system and the experiments: the experiments are carried out in closed systems; therefore, even if the water dissociates, the oxygen is still bonded to the hydrogen atoms. An important point, noted by Frost & Ballhaus (1998), in a paper about the oxidation state of the Earth's mantle, is that if the oxygen comes from the dissociation of water we need to release to the environment 3.88 moles of H_2 per m^3 of magma to yield 1.94 moles of free oxygen. We shall show in the following section that this is not a trivial issue.

The oxidation state of magmas controlled by degassing

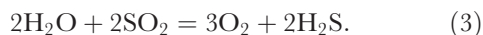
On the basis of the above discussion it is clear that the oxidation process must be driven by the degassing of hydrogen as H_2 , or combined with sulphur or chlorine to form other volatile compounds, and that this degassing process must be unusual, in contrast to the normal persistent Strombolian degassing (Allard *et al.*, 1994, 2000; Carapezza *et al.*, 2004). Carapezza *et al.* (2004) reported that the 28 December 2002 eruption began with a sudden gas release (glowing avalanche) followed by a high effusion rate lava flow, reflecting emptying of the upper conduit. Those workers also reported the rapid opening of a fracture in the Sciara del Fuoco, which triggered sudden depressurization of the magma body and anomalous gas release. It follows that this sudden depressurization is the most probable candidate to produce the high level of oxidation.

The oxidation state of most terrestrial magmas is normally between the QFM and NNO oxygen buffers. Pioneering insights were given by Sato (1969) and Carmichael *et al.* (1974). One of the first studies to model the behaviour of volatile phases in magmas was that of Gerlach & Nordlie (1975). Those workers pointed out that if the oxidation state of magmas is buffered solely by their gas phases, only restricted ranges of oxygen fugacity near the HM buffer are possible; however, if degassing of magmatic gases occurs in thermochemical equilibrium between volatiles and the melt, the oxygen fugacity of the magma can range between that of the HM and QFM buffers [for a detailed discussion of these buffers see, for example, Shi (1992)]. This shows, immediately, why it is not sufficient for the magma to be in contact with the atmosphere to reach highly oxidizing conditions. If equilibrium conditions persist and equilibrium degassing is allowed to modify the system, the oxygen fugacity will remain within the range of the QFM and HM buffers. This argument also supports the opposite hypothesis: if the system reaches an oxygen fugacity above the QFM and HM buffers, then

degassing must have occurred under non-equilibrium conditions.

In addition to water, other species in the melt can control the oxygen fugacity through degassing. In the particular case of Stromboli, Allard *et al.* (1994) have pointed out that sulphur and carbon compounds are also important. The degassing of various sulphur compounds, such as SO₂ and H₂S, is affected by oxygen fugacity and also by the interaction of the magma with water (Carmichael, 1991; Jugo *et al.*, 2005). Here we are interested in the opposite effect; that is, whether differential degassing of the volatile phases can modify the oxygen fugacity, and, if so, the extent to which this plays a role in the generation of highly oxidizing conditions at Stromboli.

By definition, in thermodynamics a non-equilibrium process is an irreversible process, which, mathematically, is equivalent to a non-continuous function representing the path of the process. The discontinuity in the pathway represents a sudden finite change in the conditions of the system. Developing this idea further, if we assume thermochemical equilibrium in the system before the sudden finite change in conditions, and consider only the effect of sulphur compounds together with the dissociation of water, equation (2) becomes



In the development of their computational model of the C–O–H–S system, Moretti *et al.* (2003) found that the equilibrium constant for equation (3) is a function of temperature:

$$\ln[k] = 8.223 - \frac{54209}{T(\text{K})}. \quad (4)$$

Combining (4) with the thermodynamic equilibrium expression for equation (3), and rearranging, we obtain

$$\log[f\text{O}_2] = \frac{\log\left[\left(\frac{f\text{SO}_2/f\text{H}_2\text{O}}{f\text{H}_2\text{S}}\right)\exp\left(8.223 - \frac{54209}{T(\text{K})}\right)\right]}{1.5} \quad (5)$$

From equation (5), it is clear that at a given temperature, the oxygen fugacity of the system is strongly linked with the fugacity of several volatile species in the melt (i.e. SO₂, H₂O, H₂S). Therefore, if the solubility of individual volatile species is different, sudden changes of the conditions that control the solubility of the volatile phases can change dramatically the value of their fugacities in equation (5). It is, therefore, possible that sudden, transient, degassing of H₂S could increase the oxygen fugacity to the value of $\log f\text{O}_2 = -0.678$ bars; however, this effect would be significant only until the magma re-equilibrated.

The processes that control transient degassing are not well understood. Different volatile species degas

at different pressures (Gerlach & Graeber, 1985; Allard *et al.*, 1994; Burton *et al.*, 2003). The converse must, therefore, also hold true—that sudden decompression of the magma chamber should initiate transient degassing.

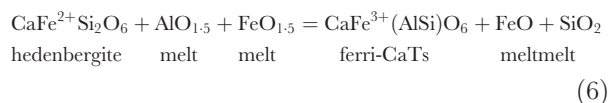
Fe³⁺/Fe²⁺ ratio in clinopyroxene

The Fe³⁺/Fe²⁺ ratio in the clinopyroxene phenocrysts from the highly oxidized samples (STR59, STR903) is higher than that in the clinopyroxene from the normal Stromboli basalts (Table 3). We now show how and why this ratio must be dependent on temperature and oxygen fugacity.

The FeO/MgO clinopyroxene–melt partition coefficient [from Baker & Egger (1987) and Sisson & Grove (1993)] ensures that the FeO/MgO ratio in the clinopyroxene depends on both temperature and the FeO/MgO ratio in the melt. The amount of FeO in the melt is, on the other hand, constrained by the oxygen fugacity because the Fe₂O₃/FeO molar ratio, following Carmichael & Ghiorso (1990) among others, is also a function of the oxygen fugacity and temperature. Clearly, the amount of Fe³⁺ in the clinopyroxene must be proportional to the availability of this species in the melt. It follows that the Fe³⁺/Fe²⁺ ratio in clinopyroxene must be dependent on temperature, the composition of the melt and oxygen fugacity.

To constrain this, we consider that Fe³⁺ can enter pyroxene in two possible ways: as (NaFe³⁺)Si₂O₆ (the aegirine or acmite end-member), or CaFe³⁺AlSiO₆ (ferri-Tschermak's molecule). Acmite is the dominant Fe³⁺ pyroxene end-member in highly alkaline magmas in which the clinopyroxene is Na-rich (Deer, *et al.*, 1997b). Although many of the Stromboli lavas are alkali-rich, they are not sodic but potassic. Furthermore, clinopyroxene compositions within the studied samples indicate that the amount of the jadeite end-member is negligible (Table 3). We therefore, assume that Fe³⁺ in the oxidized lavas enters clinopyroxene as the ferri-calcium Tschermak's molecule (ferri-CaTs), instead of Fe²⁺ as hedenbergite in the normal more reduced lavas.

Thus, we have the following reaction:



for which the equilibrium constant is

$$K_D = \gamma \left(\frac{[\text{Fe}^{3+}\text{Al}]}{[\text{Fe}^{2+}\text{Si}]} \right)^{\text{cpx}} \left(\frac{x\text{FeO}}{x\text{FeO}_{1.5}} \right)^{\text{melt}} \left(\frac{x\text{SiO}_2}{x\text{AlO}_{1.5}} \right)^{\text{melt}}. \quad (7)$$

The first term, γ , is the activity coefficient from chemical potential considerations, and has to be evaluated

experimentally. The second term is the ratio $(\text{Fe}^{3+}\text{Al})/(\text{Fe}^{2+}\text{Si})$ in the pyroxene formula, which represents the replacement of hedenbergite by the ferri-CaTs molecule. The third term is the ratio of ferrous–ferric iron in the melt, which as we have already shown, is a function of oxygen fugacity and temperature, following Sack *et al.* (1980) among others. The last term is the ratio between the concentration of silica and alumina in the melt, which is dependent on the degree of differentiation of the melt, which is itself temperature dependent.

In Fig. 8a we have plotted the relation between Al and Si contents (cations per formula unit; c.f.u.) in the clinopyroxene phenocrysts from the studied samples (both control and oxidized), from which we can conclude that the replacement of Si by Al is relatively linear and close to 1:1, suggesting that almost all of this replacement is related to the interchange ferric–ferrous iron. In Fig. 8b, the ratio $(\text{Fe}^{3+}\text{Al})/(\text{Fe}^{2+}\text{Si})$ is plotted vs Al (c.f.u. calculated on the basis of six oxygens), in cores, rims and groundmass clinopyroxene from the highly oxidized samples (STR59, STR903), the sub-liquidus (STR86), sub-solidus (STR281202c) oxidized samples and the control samples (STR47, STR4). Clearly, oxidizing conditions favour the replacement of hedenbergite by the ferri-CaTs molecule, compared with clinopyroxene formed under more reducing conditions.

Silica activity is also an important parameter in equation (7). However, although the sample with the higher bulk-rock SiO_2 content (STR59) appears to have clinopyroxene phenocrysts with a higher dispersion of $(\text{Fe}^{3+}\text{Al})/(\text{Fe}^{2+}\text{Si})$, suggesting some relation, sample STR903 contains orthopyroxene, and, therefore, must have a higher value of silica activity than sample STR59. Therefore, the relationship with silica activity remains unclear, and the control played by the silica/alumina ratio in the melt requires further investigation.

Clinopyroxene oxygen barometry

Although the $\text{Fe}^{3+}/\text{Fe}^{2+}$ (c.f.u.) ratio in clinopyroxene and oxygen fugacity cannot be directly correlated, because of the temperature and compositional dependence shown in the previous section, there is some kind of relationship indicated in Fig. 8b. Assuming a compositional range between basalt and basaltic andesite, it is possible to estimate the oxygen fugacity of the melt in which the clinopyroxene was formed, for a given temperature.

We have compiled data from published equilibrium crystallization experiments performed by Grove & Bryan (1983), Kinzler & Grove (1985), Baker & Eggler (1987), Grove & Juster (1989), Sisson & Grove (1993), Snyder *et al.* (1993), Toplis & Carroll (1995) and Sugawara (2001), in which oxygen fugacity, temperature and the composition of both clinopyroxene and melt are reported. The calculation of Fe^{3+} and Fe^{2+} in

Table 10: Calculated intrinsic oxygen fugacity using the clinopyroxene oxygen barometer method

Sample	Location	n	Mean	σ_{n-1}
STR4	core	7	1.48	0.7
STR4	middle	7	1.39	1.11
STR4	rim	6	1.62	0.74
STR4	groundmass	5	0.56	0.5
STR86	core	6	1.29	0.34
STR86	middle	4	1.33	0.96
STR86	rim	5	1.56	0.49
STR86	groundmass	4	6.32	2.26
STR47	core	10	1.51	0.83
STR47	rim	6	1.15	0.35
STR47	groundmass	3	0.89	0.2
STR281202c	core	4	0.18	0.77
STR281202c	middle	2	0.1	0.23
STR281202c	rim	6	1.12	0.97
STR281202c	groundmass	2	2.13	0.79
STR59	core	5	4.87	1.18
STR59	middle	2	2.56	1.55
STR59	rim	8	6.92	2.44
STR59	groundmass	6	8.69	1.35
STR903	core	7	2.22	0.78
STR903	middle	6	2.63	1.73
STR903	rim	5	7.72	2.12
STR903	groundmass	5	7	1.97

n , number of calculations for each sample; σ_{n-1} , standard deviation of the calculations. (See text for details.)

clinopyroxene was determined using charge balance considerations following Lindsley (1983), and the oxygen fugacity is referenced to QFM (ΔQFM) to eliminate the temperature dependence. In Fig. 8c we have plotted the $\text{Fe}^{3+}/\text{Fe}^{2+}$ (c.f.u.) ratio in clinopyroxene from the experimental dataset versus the intrinsic oxygen fugacity relative to QFM. A second-degree polynomial regression was found to be the best fit in terms of r^2 and is given in equation (8):

$$\Delta\text{QFM} = -1.801 \left(\frac{\text{Fe}^{3+}}{\text{Fe}^{2+}} \right)_{\text{cpx}}^2 + 8.753 \left(\frac{\text{Fe}^{3+}}{\text{Fe}^{2+}} \right)_{\text{cpx}} - 0.943. \quad (8)$$

The r^2 of this fit is 0.81 and the standard error is 1.036. This means that ΔQFM calculated using equation (8) has an error of ± 2 in order to fit the experimental data with 95% confidence. Although a poor fit, equation (8) is important in that it allows us to estimate the intrinsic

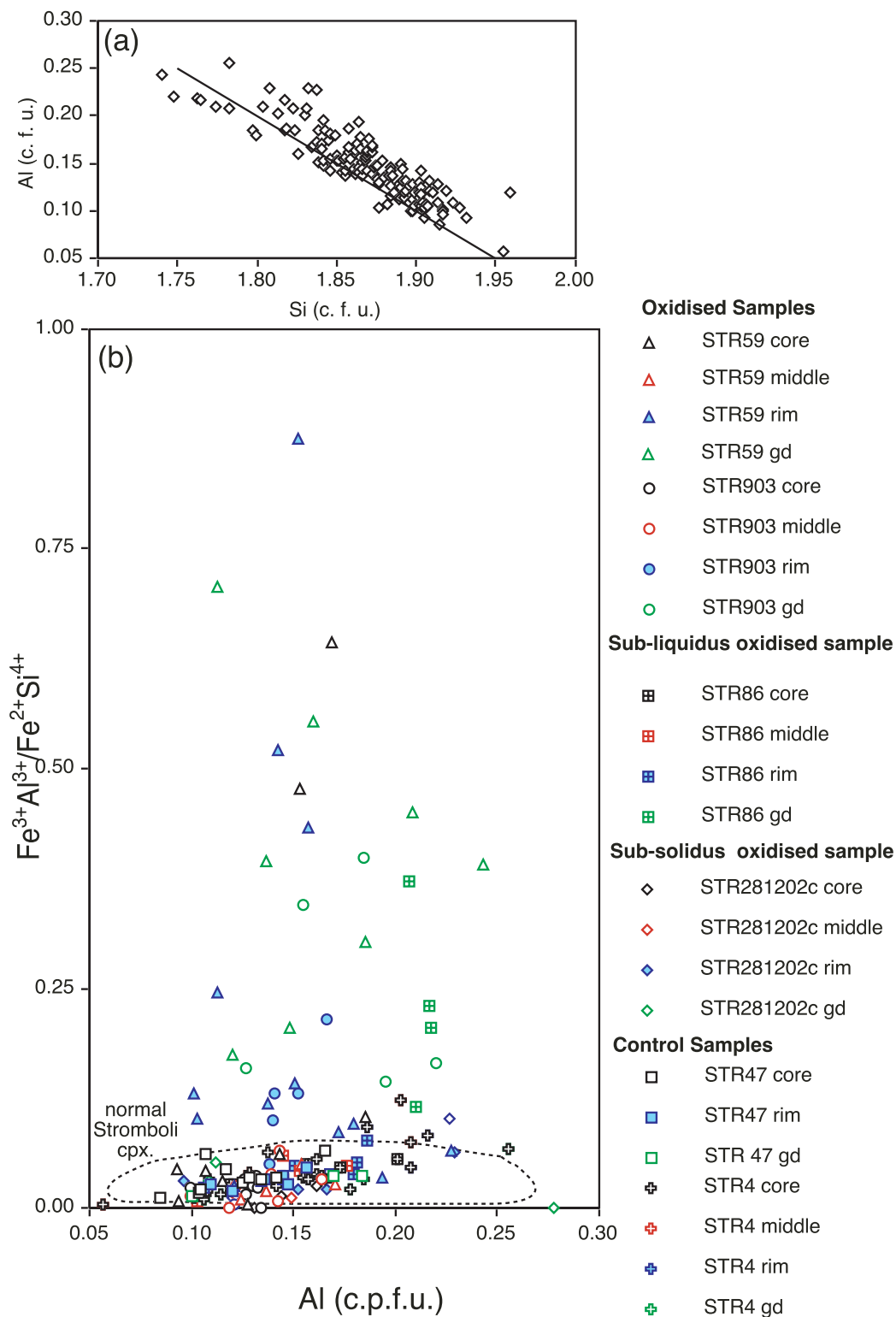


Fig. 8. (a) Variation of Al cations per formula unit (c.f.u.) vs Si (c.f.u.) in clinopyroxenes from the highly oxidized samples and the control samples, showing near 1:1 replacement of Si by Al (continuous line; see text). (b) Variation of $\text{Fe}^{3+}\text{Al}^{3+}/\text{Fe}^{2+}\text{Si}^{4+}$ (c.f.u.) vs Al (c.f.u.) for clinopyroxene phenocrysts (cores, middles and rims) and groundmass clinopyroxene in highly oxidized samples (STR59, STR903), sub-liquidus oxidized sample (STR86), sub-solidus oxidized sample (STR281202c) and control samples (STR47, STR4). (c) ΔQFM vs $\text{Fe}^{3+}/\text{Fe}^{2+}$ (c.f.u.) ratio in experimental clinopyroxenes. The line represents a second-degree polynomial fit, with $r^2 = 0.81$. (For data sources see text.)

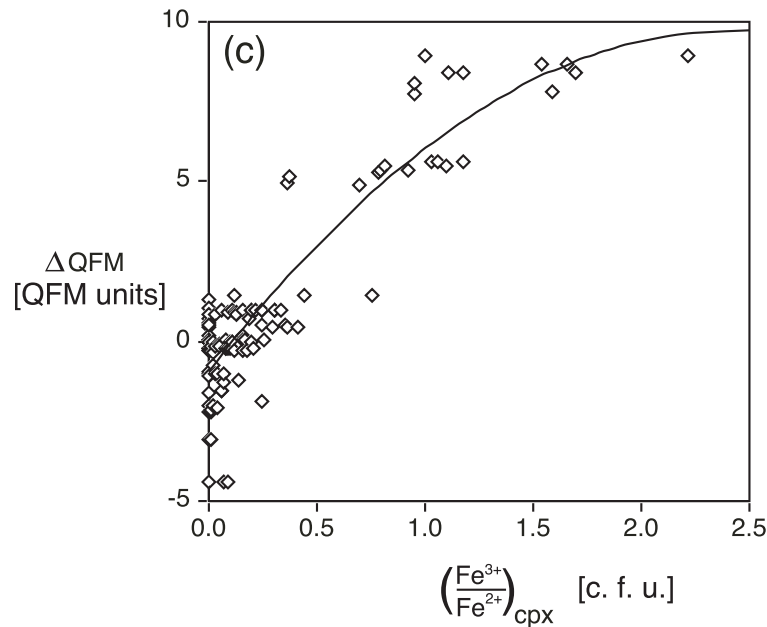


Fig. 8. Continued

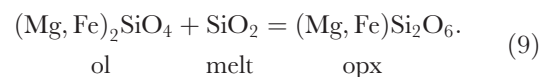
oxygen fugacity of a given magma, knowing the composition of a single clinopyroxene phenocryst or groundmass phase growing in thermochemical equilibrium with the melt.

The results of applying equation (8) to the clinopyroxene phenocrysts in the studied Stromboli samples are given in Table 10 and Fig. 9. These results are in excellent agreement with the estimation of the oxidation state of the samples based on their bulk-rock compositions (Fig. 7) using the approach of Kilinc *et al.* (1983) and Kress & Carmichael (1988). Additionally, they allow us to demonstrate that the oxidation process is not related to alteration but is a primary feature. From Fig. 9 it is clear that in sample STR86 oxidation took place before the groundmass was formed, consistent with the concept of sub-liquidus oxidation. On the other hand, in sample STR281202c, the groundmass clinopyroxene appears to have formed under normal oxidation conditions, suggesting that in this case a different oxidation process occurred in the sub-solidus state.

In the highly oxidized sample STR59 cores, rim and groundmass clinopyroxene reflect highly oxidizing conditions ($\Delta\text{QFM} > 5$), although there appears to be a fluctuation to more reducing conditions during the crystallization of the middle part of the phenocrysts. In STR903 the cores of the clinopyroxene phenocrysts record normal conditions ($\Delta\text{QFM} \approx 2$), whereas both rim and groundmass cpx record highly oxidizing conditions, suggesting that the magma was already partially crystallized when oxidation occurred.

Orthopyroxene reaction rims on olivine

As noted earlier, orthopyroxene occurs as reaction rims on Mg-rich olivine phenocrysts in sample STR903 (Fig. 2f). Cortés *et al.* (2005) explained a similar textural relationship (involving normal composition olivine phenocrysts) in lavas from the Vancori period in terms of magma mixing. In their interpretation, basaltic magma containing olivine phenocrysts was injected into a more evolved melt, resulting in the following reaction between the melt and the olivine phenocrysts:



Equation (9) implies that silica activity ($a\text{SiO}_2$) should be sufficiently high to allow reaction of the olivine phenocrysts with the melt to form orthopyroxene; $a\text{SiO}_2$ normally increases when a melt evolves from basaltic compositions to andesitic compositions, or, in the context of magma mixing, when a less evolved melt is injected into a more evolved magma. From Table 6, an origin by magma mixing is an unlikely scenario for STR903 as it has only 50 wt % SiO_2 . An alternative explanation to increase the silica activity of this melt is provided directly by the highly oxidizing conditions under which it crystallized, during which Fe is removed from the system to form Fe–Ti oxides and not silicates. These highly oxidizing conditions ensure the growth of forsterite until the silica activity is high enough to allow the crystallization of orthopyroxene.

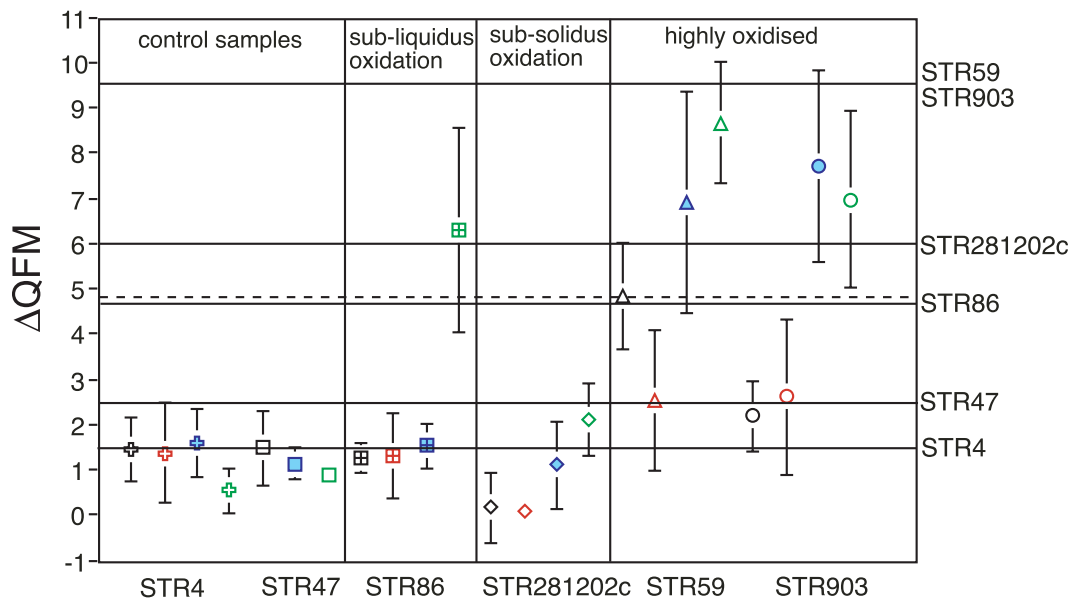


Fig. 9. Intrinsic oxygen fugacity relative to the QFM oxygen buffer (ΔQFM) calculated using the clinopyroxene oxygen geobarometer for the studied samples (see text for details). The error bars represent one standard deviation of the mean of the calculation performed for several clinopyroxenes from each sample; they do not represent the standard error of the fit represented by equation (8) (see text and Table 10 for further details). Horizontal lines represent the bulk-rock oxygen fugacity calculated using the method of Kilinc *et al.* (1983). Symbols and colours are as in Fig. 8. The dashed line represents the ΔQFM value at which Fe_2O_3/FeO (weight ratio) = 1 given the logarithmic fit from Figure 7.

Isotopic composition of the plagioclase in sample STR59

Stromboli is a classic example of an open system (Francalanci *et al.*, 1988, 1999, 2004; Bertagnini *et al.*, 2003; Cortés *et al.*, 2005) in which new inputs of magma periodically refill the magma chamber, producing mixtures of xenocrysts and phenocrysts. Often, the xenocrysts develop overgrowth rims with different compositions (Cortés *et al.*, 2005) and there is evidence of Sr isotope disequilibrium between cores and rims (Francalanci *et al.*, 2005). This has been used as evidence of magma mixing.

The potential presence of xenocrysts in the studied samples has an additional significance in the context of the oxidation process and the highly oxidized samples, because such xenocrysts could have been exposed to oxidation prior to their arrival in the magma chamber. Clearly, this scenario is irrelevant for samples exposed to sub-liquidus oxidation, because the process occurs subsequent to the formation of the phenocrysts.

Despite the fact that significant Sr isotope disequilibrium has been observed in zoned plagioclase phenocrysts from the Recent (Francalanci *et al.*, 2005) and Vancori periods of the volcano (Chertkoff *et al.*, 2004), the core to rim Sr isotope composition of the zoned plagioclase phenocrysts in sample STR59 is remarkably uniform, varying between 0.706836 ± 9 and 0.706839 ± 7 . This suggests that mixing of isotopically distinct magma batches has not occurred and that the phenocrysts are

not xenocrystic (D. Morgan, personal communication, 2005).

The role of irreversible transient degassing in generating highly oxidizing conditions in magma bodies

Following from the above discussion, it is necessary to address whether irreversible decompression can produce an oxidizing environment for a sufficiently long period of time to allow crystallization of Mg-rich olivine phenocrysts. We might expect that after a given period of time the system should return to steady-state conditions, under which a complex system of oxygen buffers will control the oxidation state of the magma. Additionally, we need to consider the possibility that sudden degassing of volatiles from the magma might trigger crystallization driven by decompression (Métrich *et al.*, 2001; Bertagnini *et al.*, 2003).

Because the transient degassing process happens at shallow levels in the magma storage system, crystallization driven by degassing, as proposed by Métrich *et al.* (2001), cannot happen because the dry and the wet liquidus coincide at low pressures. To address the more general problem of oxygen fugacity buffering beginning to act again after the system returns to steady-state conditions, we need to consider the thermodynamics of irreversible processes [e.g. the general approach of Prigogine (1967), and the approach of Fisher & Lasaga

Downloaded from <http://petrology.oxfordjournals.org/> by guest on March 23, 2015

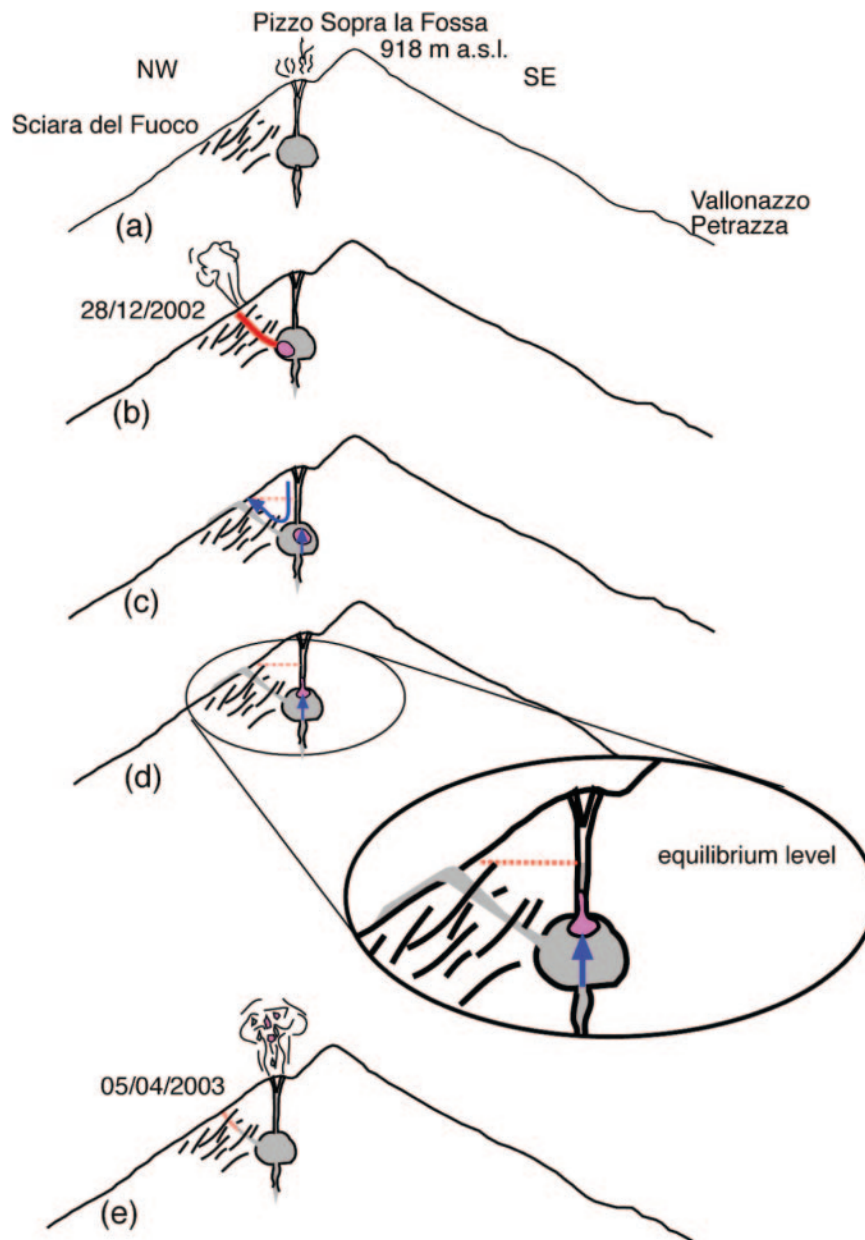


Fig. 10. Possible evolution of the Stromboli conduit system during the 2002–2003 volcanic crisis, based on Ripepe *et al.* (2005, fig. 4), the geological profile of Stromboli by Keller *et al.* (1993) and this work. (a) Normal activity of Stromboli, with equilibrium degassing of the magma and Strombolian explosions in the Pizzo area. (Note the faults in the area of Sciara del Fuoco.) (b) On 28 December 2003, a fissure was produced 100–150 m below the vents of Pizzo (Ripepe *et al.*, 2005), producing sudden decompression of the magma body and transient degassing. A portion of the magma becomes highly oxidized in the shallow chamber and is erupted through the fissure, forming a gas-rich pyroclastic flow. (c) Rapid evacuation of normal oxidation state magma from the upper part of the conduit through the fissure (Carapezza *et al.*, 2004) produces a lava flow (sample STR281202c), which becomes oxidized under sub-solidus conditions, probably by streaming of gas from the underlying volatile-rich pyroclastic flow. (d) As a result of the geometry of the fissure (sub-vertical), the lower part of the conduit rapidly becomes refilled with magma because of hydrostatic pressure constraints and begins to solidify. This magma is highly oxidized and begins to solidify, crystallizing forsterite-rich olivine. This solidified magma blocks (chokes) the upper part of the conduit (preventing eruptions from the summit craters), whereas normal oxidized lava continues to erupt through the fissure. (e) Lava flow from the Sciara del Fuoco fissure ceases and the increased internal pressure produced by a new input of gas-rich magma drives the major explosion of 5 April 2003, ejecting the highly oxidized blocks from the conduit on Ginostra (sample STR903).

(1981) applied to petrology]. Following this approach, by definition, the system (in this specific case, a batch of magma) cannot go back to its original state. Thus, it is theoretically possible that at least part of the magma body remains oxidized even after the system re-equilibrates. The ejecta should thus exhibit heterogeneities in the amount of volatiles present, their composition and in the oxidation state of the magma. Heterogeneities of this kind have been reported at a micrometre scale by Lautze & Houghton (2005) and inferred to occur at shallow levels in the Stromboli plumbing system under steady-state conditions. Consequently, it is likely that something analogous can happen under the conditions of transient degassing. The unusual Mg-rich ferromagnesian phenocrysts must have been produced in a particular, oxidized, batch of magma, which remained oxidized as a heterogeneity mingled with the normal magma, even after the magmatic system re-equilibrated. On the basis of this scenario we can understand the gap observed in the olivine compositions (Fig. 4c), the $\text{Fe}_2\text{O}_3/\text{FeO}$ weight ratio and ΔQFM (Fig. 7). Normal magmas experiencing equilibrium degassing have an $\text{Fe}_2\text{O}_3/\text{FeO}$ weight ratio <5 , an oxygen fugacity less than $+2$ in ΔQFM and olivine compositions less magnesian than Fo_{80-85} . The irreversible degassing process proposed here crosses the equilibrium boundary and moves the conditions of the system in a discontinuous step to an $\text{Fe}_2\text{O}_3/\text{FeO}$ weight ratio >10 , an oxygen fugacity of $>+9$ in ΔQFM and an olivine composition of $>\text{Fo}_{96-98}$. The discontinuity occurs precisely because the process is irreversible. The converse is also true; that is, a continuous change in any variable of the system can happen under equilibrium conditions.

A proposed model for transient degassing at Stromboli

Using the 2002–2003 volcanic crisis as a present-day example in which the oxidation process has occurred, we propose a model that can explain the conditions under which the different kinds of oxidized samples form. In Fig. 10 we present a schematic representation of the main stages of the volcanic crisis, based on the description by Ripepe *et al.* (2005). The sudden opening of a fissure on 28 December 2002 in the Sciara del Fuoco, 100–150 m below the Pizzo vents, caused transient degassing of the magma in the conduit and the oxidation of a batch of crystal-poor magma, which at that time was deeper in the system. This oxidized magma subsequently erupted through the fissure, forming the ‘glowing’ avalanche (or gas-rich pyroclastic flow). This was followed by the normal oxidation state lava that had previously filled the upper conduit of the volcano. The lava flow erupted through the fissure and flowed down the Sciara del Fuoco towards the sea (from where sample STR281202c was

collected). The sub-solidus oxidation of STR281202c was caused either by gas streaming upwards from the underlying pyroclastic deposit or by hydrothermal processes caused by interaction with sea water. The most probable geometry of the fissure is sub-vertical (M. Rosi, personal communication, 2005) ensuring that magma should partially refill the lower part of the main conduit by hydrostatic pressure after the initial draining by the fissure. Hydrostatic equilibrium in the conduit would have been rapidly re-established following the eruption of lava STR281202c from the Sciara del Fuoco fissure. This allowed highly oxidized magma from deeper in the system to rise into the conduit (but below the level of the summit craters) where it solidified over a period of weeks, crystallizing Mg-rich olivine phenocrysts. During the major explosion of 5 April 2003 the recently solidified material blocking the conduit was disrupted and lithic blocks were ejected, mainly towards Ginostra. Sample STR903 was collected from one of these blocks.

The highly oxidized Neostromboli basalt STR59, associated with the first lateral collapse of Stromboli (Vancori collapse), could have been produced by the same kind of transient degassing in an analogous way to the 2002–2003 crisis.

CONCLUSIONS

We have demonstrated that the unusual Fo_{96-97} olivine phenocrysts and the high degrees of oxidation of Stromboli samples STR59 and STR903 are primary and related to abnormal, transient, degassing of the magmatic system associated with sudden decompression. In the model proposed, this process is linked with fracturing of the volcanic edifice and possible collapse that has happened repeatedly at Stromboli for at least the past 13800 years (Vancori collapse). This model has far-reaching implications; evidence for anomalous oxidation throughout the stratigraphic sequence of the volcano could be used as an indicator of previous collapse events. Furthermore, the eruption of new magmas exhibiting anomalous oxidation could be used as a warning tool for the possibility of imminent edifice collapse.

ACKNOWLEDGEMENTS

This work was supported by the ERUPT Project ‘European Research on Understanding Processes and Timescales in Magma Systems’, funded by the European Commission (EVG1-CT2002-00058). The authors acknowledge Nicole Métrich and an anonymous reviewer for their thorough and incisive reviews of an earlier version of this manuscript. Dave Rothery, Janet Sumner and Eliza Calder are thanked for providing sample STR903, Nick Rogers for the trace element and

REE analyses of samples STR59 and STR903, Dan Morgan for the isotopic analysis of sample STR59, and Chiara Petrone for the major element analysis by wet chemistry of samples STR903 and STR281202c. Steve Blake and Ian Parkinson are acknowledged for fruitful discussions of a preliminary version of this manuscript.

SUPPLEMENTARY DATA

Supplementary data for this paper are available at *Journal of Petrology* online.

REFERENCES

- Abruzzese, D. (1935). Attività dello Stromboli dal 1930 al 1934. *Bollettino della Società Sismologica Italiana* **33**, 118–125.
- Aiuppa, A. & Federico, C. (2004). Anomalous magmatic degassing prior to the 5th April 2003 paroxysm on Stromboli. *Geophysical Research Letters* **31**, L14607, doi: 10.1029/2004GL020458.
- Allard, P., Carbonnelle, J., Métrich, N., Loyer, H. & Zettwoog, P. (1994). Sulphur output and magma degassing budget of Stromboli volcano. *Nature* **368**, 326–330.
- Allard, P., Aiuppa, A., Loyer, H., Carrot, F., Gaudry, A., Pinte, G., Michel, A. & Dongarrà, G. (2000). Acid gas and metal emission rates during long-lived basalt degassing at Stromboli volcano. *Geophysical Research Letters* **27**, 1207–1210.
- Arrighi, S. (2004). Recent eruptive history of Stromboli (Aeolian Islands, Italy) determined from high-accuracy archeomagnetic dating. *Geophysical Research Letters* **31**, L19603, doi: 10.1029/2004GL020627.
- Baker, D. R. & Eggler, D. (1987). Compositions of anhydrous and hydrous melts coexisting with plagioclase, augite and olivine or low-Ca pyroxene from 1 atm to 8 kbar: application to the Aleutian volcanic center of Atka. *American Mineralogist* **72**, 12–28.
- Baker, L. & Rutherford, M. J. (1996). The effect of dissolved water on the oxidation state of silicic melts. *Geochimica et Cosmochimica Acta* **60**, 2179–2187.
- Barberi, F., Rosi, M. & Sodi, A. (1993). Volcanic hazard assessment at Stromboli based on review of historical data. *Acta Vulcanologica* **3**, 173–187.
- Bertagnini, A., Métrich, N., Landi, P. & Rosi, M. (2003). Stromboli volcano (Aeolian Archipelago, Italy): an open window on the deep-feeding system of a steady state basaltic volcano. *Journal of Geophysical Research* **108**(B7), 2336, doi: 10.1029/2002JB002146.
- Burton, M., Allard, P., Mure, F. & Oppenheimer, C. (2003). FTIR remote sensing of fractional magma degassing at Mount Etna, Sicily. In: Oppenheimer, C., Pyle, D. M. & Barclay, J. (eds) *Volcanic Degassing*. Geological Society, London, *Special Publications* **213**, 281–293.
- Carapezza, M. L., Inguaggiato, S., Brusca, L. & Longo, M. (2004). Geochemical precursors of the activity of an open-conduit volcano: the Stromboli 2002–2003 eruptive events. *Geophysical Research Letters* **31**, L07620, doi: 10.1029/2004GL019614.
- Carmichael, I. S. E. (1991). The redox states of basic and silicic magmas: a reflection of their source regions? *Contributions to Mineralogy and Petrology* **106**, 129–141.
- Carmichael, I. S. E. & Ghiorso, M. (1990). The effect of oxygen fugacity on the redox state of natural liquid and their crystallizing phases. In: Nicholls, J. & Russell, J. K. (eds) *Modern Methods of Igneous Petrology: Understanding Magmatic Processes*. Mineralogical Society of America, *Reviews in Mineralogy* **24**, 191–212.
- Carmichael, I. S. E., Turner, F. J. & Verhoogen, J. (1974). *Igneous Petrology*. New York: McGraw–Hill, 739 pp.
- Cawthorn, R. G. & Collerson, K. D. (1974). The recalculation of pyroxene end-member parameters and the estimation of ferrous and ferric iron content from electron microprobe analyses. *American Mineralogist* **59**, 1203–1208.
- Chertkoff, D. G., Morgan, D. J., Francalanci, L., Davidson, J., Jerram, D. A., Nowell, G. M. & Pearson, D. G. (2004). Textural and Sr isotopic analysis of plagioclase phenocrysts from Stromboli volcano (Aeolian Islands): evidence for open-system magmatic processes in the evolution and eruption of the Vancori series. European Geosciences Union, General Assembly, Nice, 01089, EGU04-A-01089.
- Cortés, J. A., Wilson, M., Condliffe, E., Francalanci, L. & Chertkoff, D. G. (2005). The evolution of the magmatic system of Stromboli Volcano during the Vancori period (26–13.8 ky). *Journal of Volcanology and Geothermal Research* **147**(1–2), 1–38. doi: 10.1016/j.jvolgeores.2005.03.005.
- Cressey, G. & Howie, R. A. (2005). Minerals; olivines. In: Selley, R. C., Cocks, L. R. M. & Plimer, I. R. (eds) *Encyclopedia of Geology, Volume 3*. Amsterdam: Elsevier, pp. 557–561.
- Deer, W. A., Howie, R. A. & Zussman, J. (1997a). *Orthosilicates*. London: Geological Society, 919 pp.
- Deer, W. A., Howie, R. A. & Zussman, J. (1997b). *Single-Chain Silicates*. London: Geological Society, 668 pp.
- Ferrari, L. & Manetti, P. (1993). Geodynamic framework of the Tyrrhenian volcanism: a review. *Acta Vulcanologica* **3**, 1–9.
- Fisher, G. W. & Lasaga, A. C. (1981). Irreversible thermodynamics in petrology. In: Lasaga, A. C. & Kirkpatrick, R. J. (eds) *Kinetics of Geochemical Processes*. Mineralogical Society of America, *Reviews in Mineralogy* **8**, 171–207.
- Francalanci, L. (1993). Mineral chemistry of Stromboli volcanics as indicator of magmatic processes. *Acta Vulcanologica* **3**, 99–113.
- Francalanci, L., Barbieri, M., Manetti, P., Peccerillo, A. & Tolomeo, L. (1988). Sr-isotopic systematics in volcanic rocks from the island of Stromboli (Aeolian arc). *Chemical Geology* **73**, 164–180.
- Francalanci, L., Manetti, P. & Peccerillo, A. (1989). Volcanological and magmatological evolution of Stromboli volcano (Aeolian islands): the roles of fractional crystallisation, magma mixing, crustal contamination and source heterogeneity. *Bulletin of Volcanology* **51**, 355–378.
- Francalanci, L., Manetti, P., Peccerillo, A. & Keller, J. (1993). Magmatological evolution of the Stromboli volcano (Aeolian Arc, Italy): inferences from major and trace element and Sr-isotopic composition of lavas and pyroclastic rocks. *Acta Vulcanologica* **3**, 127–151.
- Francalanci, L., Tommasini, S., Conticelli, S. & Davies, G. (1999). Sr isotope evidence for short magma residence time for the 20th century activity at Stromboli volcano, Italy. *Earth and Planetary Science Letters* **167**, 61–69.
- Francalanci, L., Tommasini, S. & Conticelli, S. (2004). The volcanic activity of Stromboli in the 1906–1998 A.D. period: mineralogical, geochemical and isotope data relevant to the understanding of the plumbing system. *Journal of Volcanology and Geothermal Research* **131**, 179–211.
- Francalanci, L., Davies, G. R., Lustenhouwer, W., Tommasini, S., Mason, P. R. D. & Conticelli, S. (2005). Intra-grain Sr isotope evidence for crystal recycling and multiple magma reservoirs in the recent activity of Stromboli Volcano, Southern Italy. *Journal of Petrology* **46**, 1997–2021, doi: 10.1093/petrology/egi045.
- Frost, C. D. & Ballhaus, C. (1998). Comment on ‘Constraints on the origin of the oxidation state of mantle overlying subduction zones: an example from Simcoe, Washington, USA’ by A. D. Brandon and D. S. Draper. *Geochimica et Cosmochimica Acta* **62**, 329–331.

- Gaillard, F., Scaillet, B., Pichavant, M. & Bény, J. M. (2001). The effect of water and f_{O_2} on the ferric–ferrous ratio of silicic melts. *Chemical Geology* **174**, 255–273.
- Gerlach, T. M. & Graeber, E. J. (1985). Volatile budget of Kilauea Volcano. *Nature* **313**, 273–277.
- Gerlach, T. M. & Nordlie, B. E. (1975). The C–O–H–S gaseous system, Part I: Composition limits and trends in basaltic cases. *American Journal of Science* **275**, 353–376.
- Grove, T. L. & Bryan, W. B. (1983). Fractionation of pyroxene–phyric MORB at low pressure: an experimental study. *Contributions to Mineralogy and Petrology* **84**, 293–309.
- Grove, T. L. & Juster, T. C. (1989). Experimental investigations of low-Ca pyroxene stability and olivine–pyroxene–liquid equilibria at 1 atm in natural basaltic and andesitic liquids. *Contributions to Mineralogy and Petrology* **103**, 287–305.
- Haggerty, E. & Baker, I. (1967). The alteration of olivine in basaltic and associated lavas. Part I: High temperature alteration. *Contributions to Mineralogy and Petrology* **16**, 233–257.
- Honnorez, J. & Keller, J. (1968). Xenolithe in vulkanischen Gesteiner der Aoliaschen Inseln (Sizilien). *Geologische Rundschau* **57**, 719–736.
- Hornig-Kjarsgaard, I., Keller, J., Koberski, U., Stadlbauer, E., Francalanci, L. & Lenhart, R. (1993). Geology, stratigraphy and volcanological evolution of the island of Stromboli, Aeolian arc, Italy. *Acta Vulcanologica* **3**, 21–68.
- Huebner, J. S. & Sato, M. (1970). The oxygen and temperature relationships of manganese and nickel oxide buffers. *American Mineralogist* **55**, 934–952.
- Jugo, P., Luth, R. W. & Richards, J. P. (2005). Experimental data on the speciation of sulfur as a function of oxygen fugacity in basaltic melts. *Geochimica et Cosmochimica Acta* **69**(2), 497–503, doi: 10.1016/j.gca.2004.07.011.
- Keller, J., Hornig-Kjarsgaard, I., Koberski, U., Stadlbauer, E. & Lenhart, R. (1993). Geological map of the island of Stromboli—scale 1:10 000. *Acta Vulcanologica* **3**, appendix.
- Kilinc, A., Carmichael, I. S. E., Rivers, M. L. & Sack, R. O. (1983). The ferric–ferrous ratio of natural silicate liquids equilibrated in air. *Contributions to Mineralogy and Petrology* **83**, 136–140.
- Kinzler, R. J. & Grove, T. L. (1985). Primary magmas of mid-ocean ridge basalts. 1. Experiments and methods. *Journal of Geophysical Research* **97**, 6885–6906.
- Kress, V. C. & Carmichael, I. S. E. (1988). Stoichiometry of the iron oxidation reaction in silicate melts. *American Mineralogist* **73**, 1267–1274.
- Lautze, N. C. & Houghton, B. F. (2005). Physical mingling of magma and complex eruption dynamics in the shallow conduit at Stromboli volcano, Italy. *Geology* **22**, 425–428.
- Lindsley, D. H. (1983). Pyroxene thermometry. *American Mineralogist* **68**, 477–493.
- Loucks, R. (1996). A precise olivine–augite Mg–Fe-exchange geothermometer. *Contributions to Mineralogy and Petrology* **125**, 140–150.
- McDonough, W. F. & Sun, S. S. (1995). The composition of the Earth. *Chemical Geology* **120**, 223–253.
- Métrich, N., Bertagnini, A., Landi, P. & Rosi, M. (2001). Crystallization driven by decompression and water loss at Stromboli Volcano (Aeolian Islands, Italy). *Journal of Petrology* **42**, 1471–1490.
- Moore, G., Righter, K. & Carmichael, I. S. E. (1995). The effect of dissolved water on the oxidation state of iron in natural silicate liquids. *Contributions to Mineralogy and Petrology* **120**, 170–179.
- Moretti, R., Papale, P. & Ottonello, G. (2003). A model for the saturation of C–O–H–S fluids in silicate melts. In: Oppenheimer, C., Pyle, D. M. & Barclay, J. (eds) *Volcanic Degassing*. Geological Society, London, Special Publications **213**, 81–101.
- Myers, J. & Eugster, H. P. (1983). The system Fe–Si–O oxygen buffer calibration to 1500 K. *Contributions to Mineralogy and Petrology* **82**, 75–90.
- O'Neill, H. S. C. (1987). Quartz–fayalite–iron and quartz–fayalite–magnetite equilibria and the free energy of formation of fayalite (Fe_2SiO_4) and magnetite (Fe_3O_4). *American Mineralogist* **72**, 65–75.
- Peccerillo, A. & Taylor, S. R. (1976). Geochemistry of Eocene calc-alkaline volcanic rocks from the Kastamonu area, northern Turkey. *Contributions to Mineralogy and Petrology* **58**, 63–81.
- Prigogine, I. (1967). *Thermodynamics of Irreversible Processes*. New York: John Wiley, 164 pp.
- Renzulli, A., Serri, G., Santi, P., Mattioli, M. & Holm, P. M. (2001). Origin of high-silica liquids at Stromboli volcano (Aeolian island, Italy) inferred from crustal xenoliths. *Bulletin of Volcanology* **62**, 400–419.
- Renzulli, A., Tribaudino, M., Salvioli-Mariani, E., Serri, G. & Holm, P. M. (2003). Cordierite–anorthoclase hornfels xenoliths in Stromboli lavas (Aeolian Islands, Sicily): an example of a fast cooled contact aureole. *European Journal of Mineralogy* **15**, 665–679.
- Revil, A., Finizola, A., Sortino, F. & Ripepe, M. (2004). Geophysical investigations at Stromboli volcano, Italy: implications for ground water flow and paroxysmal activity. *Geophysical Journal International* **157**, 426–440, doi: 10.1111/j.1365-246X.2004.02181.x.
- Ripepe, M., Marchetti, E., Ulivieri, G., Harris, A., Dehn, J., Burton, M., Caltabiano, T. & Salerno, G. (2005). Effusive to explosive transition during the 2003 eruption of Stromboli volcano. *Geology* **33**(5), 341–344, doi: 10.1130/G21173.1.
- Roeder, P. L. & Emslie, R. F. (1970). Olivine–liquid equilibrium. *Contributions to Mineralogy and Petrology* **29**, 275–289.
- Rosi, M., Bertagnini, A., Landi, P. (2000). Onset of the persistent activity at Stromboli Volcano (Italy). *Bulletin of Volcanology* **62**, 294–300.
- Sack, R. O. & Ghiorsio, M. (1991). An internally consistent model for the thermodynamic properties of Fe–Mg–titanomagnetite–aluminates spinels. *Contributions to Mineralogy and Petrology* **106**, 474–505.
- Sack, R. O., Carmichael, I. S. E., Rivers, M. L. & Ghiorsio, M. (1980). Ferric–ferrous equilibria in natural silicate liquids at 1 bar. *Contributions to Mineralogy and Petrology* **75**, 369–376.
- Sato, M. (1969). *Oxygen Fugacity of Basaltic Magma at Various Stages of Crystallization*. Geological Society of America, Special Papers **264**, 1969 pp.
- Shi, P. (1992). Fluid fugacities and phase equilibria in the Fe–Si–O–H–S system. *American Mineralogist* **77**, 1050–1066.
- Sigurdsson, H. & Brown, G. M. (1970). An unusual enstatite–forsterite basalt from Kolbeinsey Island, north of Iceland. *Journal of Petrology* **11**, 205–220.
- Sisson, T. W. & Grove, T. L. (1993). Experimental investigations of the role of H_2O in calc-alkaline differentiation and subduction zone magmatism. *Contributions to Mineralogy and Petrology* **113**, 143–166.
- Snyder, D., Carmichael, I. S. E. & Wiebe, R. A. (1993). Experimental study of liquid evolution in an Fe rich, layered mafic intrusion: constraints of Fe–Ti oxide precipitation on the T – f_{O_2} and T – r path of tholeiitic magmas. *Contributions to Mineralogy and Petrology* **113**, 73–86.
- Stolper, E. (1982). The speciation of water in silicate melts. *Geochimica et Cosmochimica Acta* **46**, 2609–2620.
- Sugawara, T. (2001). Ferric iron partitioning between plagioclase and silicate liquid: thermodynamics and petrological applications. *Contributions to Mineralogy and Petrology* **141**, 659–686.
- Tibaldi, A. (2001). Multiple sector collapses at Stromboli volcano, Italy: how they work. *Bulletin of Volcanology* **63**, 112–125.
- Tibaldi, A., Pasquarè, G., Francalanci, L. & Garduño, V. H. (1994). Collapse type and recurrence at Stromboli volcano, associated

- volcanic activity, and sea level changes. *International Symposium on Large Explosive Eruptions, the Problems of Eruption Forecasting and Warning: Limits and Possibilities. Accademia Nazionale Dei Lincei, Atti Convegni Lincei* **112**, 143–151.
- Tibaldi, A., Coarazzato, C., Apuani, T. & Cancelli, A. (2003). Deformation at Stromboli volcano (Italy) revealed by rock mechanisms and structural geology. *Tectonophysics* **361**, 187–204.
- Toplis, M. J. & Carroll, M. R. (1995). An experimental study of the influence of oxygen fugacity on Fe–Ti oxide stability, phase relations, and mineral–melt equilibria in ferro-basaltic systems. *Journal of Petrology* **36**(5), 1137–1170.
- Trommsdorff, V. & Evans, B. W. (1972). Progressive metamorphism of antigorite schist in the Bergell Tonalite aureole (Italy). *American Journal of Science* **272**, 423–437.
- Trommsdorff, V. & Evans, B. W. (1974). Alpine metamorphism of peridotitic rocks. *Schweizerische Mineralogische und Petrographische Mitteilungen* **54**, 333–352.
- Trommsdorff, V., López Sánchez-Vizcaíno, V., Gómez-Pugnaire, M. T. & Müntener, O. (1998). High pressure breakdown of antigorite to spinifex-textured olivine and orthopyroxene. *Contributions to Mineralogy and Petrology* **132**, 139–148.
- Wager, L. R. & Brown, G. M. (1967). *Layered Igneous Rocks*. Edinburgh: Oliver & Boyd, 588 pp.